HHS Public Access

Author manuscript

Neurobiol Dis. Author manuscript; available in PMC 2023 September 27.

Published in final edited form as:

Neurobiol Dis. 2023 August ; 184: 106196. doi:10.1016/j.nbd.2023.106196.

A 14-day pulse of PLX5622 modifies α-synucleinopathy in preformed fibril-infused aged mice of both sexes

Tarun N. Bhatia[a], **Anuj S. Jamenis**[a], **Muslim Abbas**[a], **Rachel N. Clark**[a], **Kristin M. Miner**[a], **Manisha N. Chandwani**[a], **Roxanne E. Kim**[a], **William Hilinski**[b], **Lauren A. O'Donnell**[a], **Kelvin C. Luk**[c], **Yejie Shi**[d,e], **Xiaoming Hu**[d,e], **Jun Chen**[d,e], **Jeffrey L. Brodsky**[f], **Rehana K. Leak**[a,*]

[a]Graduate School of Pharmaceutical Sciences, Duquesne University, Pittsburgh, PA, USA

[b]B&B Microscopes, Olympus Corporation, Pittsburgh, PA, USA

[c]Dept. of Pathology and Laboratory Medicine, University of Pennsylvania, Philadelphia, PA, USA

[d]Geriatric Research, Education and Clinical Center, Veterans Affairs Pittsburgh Health Care System, Pittsburgh, PA, USA

[e]Pittsburgh Institute of Brain Disorders & Recovery and Department of Neurology, University of Pittsburgh School of Medicine, Pittsburgh, PA, USA

[f]Dept. of Biological Sciences, University of Pittsburgh, Pittsburgh, PA, USA

Abstract

Reactive microglia are observed with aging and in Lewy body disorders, including within the olfactory bulb of men with Parkinson's disease. However, the functional impact of microglia in these disorders is still debated. Resetting these reactive cells by a brief dietary pulse of the colony-stimulating factor 1 receptor (CSF1R) inhibitor PLX5622 may hold therapeutic potential against Lewy-related pathologies. To our knowledge, withdrawal of PLX5622 after short-term exposure has not been tested in the preformed α-synuclein fibril (PFF) model, including in aged mice of both sexes. Compared to aged female mice, we report that aged males on the control diet showed higher numbers of phosphorylated α-synuclein^{+} inclusions in the limbic rhinencephalon after PFFs were injected in the posterior olfactory bulb. However, aged females displayed larger inclusion sizes compared to males. Short-term (14-day) dietary exposure to PLX5622 followed by control chow reduced inclusion numbers and levels of insoluble α-synuclein in aged males —but not females—and unexpectedly *raised* inclusion sizes in both sexes. Transient delivery of PLX5622 also improved spatial reference memory in PFF-infused aged mice, as evidenced by an increase in novel arm entries in a Y-maze. Superior memory was positively correlated

*Corresponding author at: Graduate School of Pharmaceutical Sciences, Duquesne University, 600 Forbes Ave, Pittsburgh, PA 15282, USA., leakr@duq.edu (R.K. Leak).

Authors' contributions

Experimental design, data graphing, and biostatistical analyses: TNB, RKL. Experimentation: TNB, RNC, ASJ, MA, KMM, MNC, RK. Image analyses: TNB, RNC, MA, ASJ, RK, WH. Writing: TNB, RKL. Revisions: JLB, ASJ, KMM, RNC. Scientific feedback: JLB, KCL, YS, XH, LOD, and JC. Supervision and mentoring: RKL.

Declaration of Competing Interest

The authors have no competing interests to declare.

Supplementary data to this article can be found online at https://doi.org/10.1016/j.nbd.2023.106196.

with inclusion sizes but negatively correlated with inclusion numbers. Although we caution that PLX5622 delivery must be tested further in models of α-synucleinopathy, our data suggest that larger-sized—but fewer—α-synucleinopathic structures are associated with better neurological outcomes in PFF-infused aged mice.

Keywords

Microglia; Lewy body; Synuclein; Dementia; Neurodegeneration; Parkinson's disease; Preformed fibril; Sex; PLX5622; Olfactory bulb

1. Introduction

Microglia are believed to switch from neuroprotective to toxic phenotypes as neurological diseases advance from early to late stages (Halliday and Stevens, 2011; Harms et al., 2021; Weiss et al., 2022). In Lewy body disorders, microglia become reactive prior to the emergence of α-synucleinopathic inclusions and remain in a reactive state until autopsy (McGeer et al., 1987; McGeer et al., 1988; Olanow et al., 2019). However, human postmortem data cannot readily establish if microglia mitigate, worsen, or exert no effects on Lewy-related pathologies. Thus, the goal of the present report was to test if ablation of microglia followed by repopulation of the microglial niche would moderate the histological, biochemical, and neurological sequelae of experimental Lewy body disease.

According to experimental work, microglial reactivity is enhanced with parkinsonism-inducing toxicants (Dai et al., 2012; Klusa et al., 2010; Swarnkar et al., 2013; Zhang et al., 2021b) and with preformed fibrils (PFFs) synthesized from recombinant α-synuclein (Duffy et al., 2018b; Harms et al., 2017; Stoll and Sortwell, 2022; Thakur et al., 2017; Verma et al., 2021). PFF-induced microgliosis has also been shown to precede neuronal loss in animal models (Duffy et al., 2018b). In addition, microglia may harbor α-synuclein when surrounding inclusion-bearing neurons (Barth et al., 2021; Tanriover et al., 2020), and may thus be carriers, and not only "cleaners" of α-synuclein, possibly spreading aggregates *via* exosomes (Guo et al., 2020; Xia et al., 2019). An excess of (or aggregated) α-synuclein can also impede microglial phagocytosis (Bido et al., 2021; Haenseler et al., 2017; Park et al., 2008). In contrast, recent work suggests that α-synuclein-burdened microglia form connections with healthier microglia, perhaps to share the handling and autophagic clearance of α-synuclein (Choi et al., 2020; Scheiblich et al., 2021). Furthermore, ~80% loss of microglia exacerbates the cell-to-cell transfer of α-synuclein *in vivo* (George et al., 2019). It is therefore likely that microglia assume polymorphic phenotypes in response to proteostatic challenges and are not unidimensional in impact.

The olfactory bulb (OB) and anterior olfactory nuclei (AON) develop Lewy pathology in early stages of Lewy body disorders (Attems et al., 2014; Attems et al., 2021; Beach et al., 2009a; Beach et al., 2009b; Braak et al., 2003; Pearce et al., 1995). In the AON of PD subjects, almost as many microglia as neurons harbor α-synuclein^{+} inclusions (Stevenson et al., 2020). The human OB also displays more microgliosis in males than females with Parkinson's disease (Flores-Cuadrado et al., 2021), and yet, the functional impact of biological sex has not been systematically tested in most of the preclinical work

on Lewy body disorders. In contrast, sex differences in microglial anatomy and physiology are well established (Han et al., 2021; Hanamsagar and Bilbo, 2016; Kodama and Gan, 2019; Lenz and McCarthy, 2015; Osborne et al., 2018; Villa et al., 2019; Yanguas-Casás, 2020). For example, male mice display greater numbers of microglia at early developmental stages, and male microglia may have better phagocytic and antigen presentation capacities (Guneykaya et al., 2018; VanRyzin et al., 2019). Microglial sex differences in rodents may be critical for male sex behaviors, masculinization, and brain sexual differentiation, and may be driven by the prenatal surge in testosterone (Han et al., 2021; Hanamsagar et al., 2017; Lenz et al., 2013; Nelson et al., 2019). Sex differences in microglia are maintained even after harvest and *in vitro* culturing, in the absence of hormonal cues (Villa et al., 2018), and microglia maintain their sex phenotype, gene expression profiles, and functional effects when transplanted into the brains of the opposite sex (Villa et al., 2018). As microglia are long-lived cells (Fuger et al., 2017; Reu et al., 2017), it is conceivable that sexual dimorphisms in these cells induced by perinatal exposure to sex steroids contribute to sex-biased emergence of neurological diseases later in life. However, the functional impact of male *vs.* female microglia on Lewy-related pathologies is unclear.

During their long lifespans, aged microglia become inflamed, less motile, produce more free radicals, and show impaired phagocytosis (Angelova and Brown, 2019). In dementia with Lewy bodies (DLB), microglia show dystrophic changes, including process fragmentation, deramification, and beading (Bachstetter et al., 2015), perhaps reflecting cellular senescence (Streit et al., 2004; Streit and Xue, 2016). Experimental attempts to mitigate this aging (or diseased) microglial phenotype include inhibition of the colony stimulating factor 1 receptor (CSF1R), which regulates myeloid lineage cells and is vital for microglial survival (Elmore et al., 2014). However, recent work shows that the *long-term* loss of microglia (for two or six months) with the CSF1R inhibitor PLX3397 did not affect inclusion formation or dopaminergic neuron loss after PFFs were infused into the striata of young male rats (Stoll et al., 2023). In contrast, a short-duration pharmacologic treatment with the orally bioavailable CSF1R antagonist, PLX5622, was shown to elicit microglial repopulation, reset microglial morphologies, improve cognition and long-term potentiation, and restore expression of genes involved in cytoskeletal remodeling, axon growth, synaptic function, microtubule transport, and neurotransmitter release in aging mice (Elmore et al., 2018). Apart from aging, this pulsatile CSF1R inhibition strategy to repopulate the microglial niche has also exerted beneficial effects in models of intracerebral hemorrhage (Li et al., 2022), inflammation (Coleman Jr. et al., 2020; Rice et al., 2017), stroke (Barca et al., 2022), traumatic brain injury (Henry et al., 2020; Willis et al., 2020), toxicant-induced parkinsonism (Li et al., 2021), and Alzheimer's disease (Johnson et al., 2023). At least to our knowledge, short-term CSF1R inhibition with a pulse of dietary PLX5622 followed by withdrawal has not yet been tested in the PFF model—particularly in aged mice or as a function of biological sex.

To fill the aforementioned gaps, we used a mouse model of Lewy body disease, in which the OB is infused with PFFs (Mason et al., 2016; Mason et al., 2019; Rey et al., 2016; Rey et al., 2018). Previously, we found that PFF infusions targeted to the rear of the OB (*i.e.*, centered in the bulbar AON) lead to limbic inclusions that are immunoreactive for phosphorylated α-synuclein (pSer129) and ubiquitin, and are stained with the Proteostat dye

for amyloid protein aggregations (Bhatia et al., 2021; Mason et al., 2016; Mason et al., 2019; Miner et al., 2022). Thus, we leveraged our mouse model to test the hypothesis that transient dietary exposure to PLX5622 would mitigate limbic α-synucleinopathy in aged mice of both sexes. We chose a short delivery paradigm (14-day) of the CSF1R inhibitor, PLX5622, based on brain penetrability (~20% for PLX5622 *vs.* ~5% for PLX3397) and on-target selectivity (10-fold more than PLX3397) (Elmore et al., 2014; Liu et al., 2019; Spangenberg et al., 2019). PLX5622 has a lower molecular weight, higher lipophilicity and better cell permeability than PLX3397 (Spangenberg et al., 2019). We report that a two-week pulse of dietary PLX5622 followed by seven weeks of withdrawal improved histological and biochemical measures of limbic α-synucleinopathy, and also improved spatial reference memory.

2. Methods

For details on behavior assays, sequential extraction, flow cytometric analyses, *in vitro* primary hippocampal neuron/microglia cocultures, immunostaining, and image analyses techniques, please see the supplemental files.

2.1. Use of outbred mice and rats for in vivo and in vitro work

We raised outbred CD-1 mice and Sprague-Dawley rats, and regularly refreshed the colony with breeders from external vendors (Charles River, Wilmington, MA and Hilltop Lab Animals, Scottdale, PA). CD-1 mice are an outbred strain and different from CD1 receptor-deficient mice with knockout of Cd1d1/Cd1d2 loci (Hong et al., 1999). CD-1 mice offer the advantage of greater genetic variability than inbred mouse strains such as C57 and are therefore useful for translating findings to the diverse human population (Aldinger et al., 2009; Hsieh et al., 2017). All animal work was performed with prior approval by the Duquesne University IACUC. Animals lived in a 12/12 light cycle in the Duquesne University Animal Care Facility and were provided with free access to food and UV-disinfected water.

2.2. Delivery of the CSF1R inhibitor, PLX5622, and stereotaxic brain surgeries

The CSF1R inhibitor, PLX5622 (Chemgood, Glen Allen, VA), was prepared at 1200 mg/kg in the AIN-76A Rodent Diet (Research Diets, Inc., New Brunswick, NJ) (Dagher et al., 2015; Spangenberg et al., 2019; Zhang et al., 2019). Male and female aged CD-1 mice (18 months old; $n = 20$ per sex) were randomized into two equal groups; half were fed the PLX5622-containing diet and the other half received the control AIN-76A diet for two weeks. Bilateral stereotaxic infusions of PFFs were centered in the dorsal subdivision of the AON after seven days of initiation of the PLX5622-containing diet, as described below. Two weeks after initiating the diet (or one week after PFF infusions), standard rodent chow was delivered for an additional seven weeks (timeline in Fig. 1a).

To confirm microglia depletion by flow cytometry, 3–4 month-old male and female CD-1 mice ($n = 22$ per sex) were randomized and administered the PLX5622-containing diet ($n = 8$ per sex) or control AIN-76A diet ($n = 8$ per sex) for two weeks. To assess microglia repopulation by flow cytometry, the diet was reverted to standard rodent chow for an

additional seven weeks (n = 6 per sex). The latter work was completed in young mice because we were unable to acquire additional sex-matched 18 month-old CD-1 mice.

Stereotaxic coordinates were tested by performing practice injections with blue food dye in spare mice of the same age and sex, as CD-1 mice are larger than C57 mice used for brain atlases. Thus, bilateral injections of one microliter of PBS or 5 μg of PFFs (in 1 μL of PBS) were performed in the bulbar AON of 18-month-old male and female mice at AP + 4.0 mm, ML+/− 1.0 mm, and DV - 3.0 mm from Bregma (from top of skull rather than dura mater). PBS infusions were performed on 18 month-old mice to evaluate PFF-induced impairments in reference memory (Fig. 2; n = 9 mice) and to evaluate the nonionic detergent-insolubility of α-synuclein (Fig. 3; n = 18 mice).

PFFs were obtained from the Luk lab at the University of Pennsylvania and prepared as before (Luk et al., 2009; Luk et al., 2012; Volpicelli-Daley et al., 2011; Volpicelli-Daley et al., 2014). The PFF preparation contained 0.11 picograms LPS per microgram protein (communication from Dr. Luk). PFFs were sonicated in a waterbath (Bransonic series model M1800, Branson Ultrasonics Corporation, Danbury, CT) for 60 mins immediately prior to use, as described in our prior work (Bhatia et al., 2021; Mason et al., 2016; Mason et al., 2019; Miner et al., 2022; Nouraei et al., 2018). Our sonication protocol results in a mean fibril length of 39.8 nm and a median length of 35.2 nm by transmission electron microscopy [quantified from images shown in (Mason et al., 2016)].

Mice were anesthetized with 2 to 2.5% isoflurane, placed on a microwave-heated pad, stabilized in a stereotaxic frame (Kopf Instruments, Tujunga, CA). Scalps were shaved prior to incision, disinfected with betadine and 70% isopropyl alcohol, and the infusions were performed using a Hamilton syringe (80,085, Hamilton Company, Reno, NV), attached to a motorized injection pump (Stoelting, Wood Dale, IL) at a rate of 0.25 μL/min. Following a rest period of ~3–4 min, the needle was gradually withdrawn from the burr hole. Mice were injected subcutaneously with 0.05 mg/kg buprenorphine for pain relief and placed on an electric heating pad until complete recovery of ambulation and righting reflexes. Immediately after the surgery and for the next 3 days, topical 2% lidocaine ointment was applied at the incision site.

One PLX5622-fed aged male mouse and one PLX5622-fed aged female mouse were euthanized early due to age-related dermatitis and an abdominal abscess, respectively. One PBS-injected aged male and one PBS-injected aged female mouse from the PLX5622 cohort were euthanized early due to severe weight loss and a tumor, respectively. All test-specific exclusion criteria are described in the figure legends as well as supplemental files.

2.3. Detection of pSer129 and optimization of tyramide-based signal amplification

For studies examining pSer129, we optimized the Tyramide Signal Amplification (TSA) technique (Biotium, Fremont, CA) to improve the signal-to-noise ratio of pSer129 immunolabel in the aged mouse brains, partly based on prior work (Delic et al., 2018; Killinger et al., 2023). Note that the EP1536Y anti-pSer129 antibody that we have used in all our *in vivo* work is the best commercially available option to detect α-synucleinopathic aggregates (Delic et al., 2018; Lashuel et al., 2022). Thus, we performed a series of

experiments to confirm that TSA improves the detection of pSer129 with EP1536Y in PFF-infused mice (Fig. S1–3).

First, we applied various dilutions of the pSer129 antibody with TSA on sections from the contralateral hemisphere of 17-month-old mice injected unilaterally in the OB/AON with PFFs three months earlier [tissue was stored at −20 °C in cryoprotectant from prior work (Mason et al., 2016)]. Contralateral tissues were chosen to avoid a high density of immunolabel and plateauing of the signal (Fig. S1). Notably, diluting the primary antibody further than 1:1000 led to *far fewer* neuritic $pSer129^+$ inclusions in the piriform cortex, amygdala, and hippocampus (arrows in Fig. S1b *versus* c) and, therefore, we proceeded with the 1:1000 dilution.

Second, we tested if antigen retrieval with sodium citrate or sodium borohydride ($NaBH_4$) would further improve the TSA staining, and we compared normal goat serum (NGS), bovine serum albumin (BSA), and the LI-COR Intercept Blocking Buffer, all run in parallel (Fig. S2). TSA led to higher immunolabeling, as expected (compare sections labeled “TSA” with sections labeled “Control AF_{555}” in Fig. S2e). Indeed, the Control AF_{555} group did not show any immunolabeling at the same exposure settings and was therefore artificially brightened (with cell-Sens fixed-scaling settings) in an additional panel for illustration purposes (see staggered sections of Fig. S2e).

Finally, we repeated the TSA experiments to confirm if antigen retrieval with sodium citrate reproducibly improved TSA immunostaining (Fig. S3), but the antigen retrieval increased background noise throughout the brain section (Fig. S3c–l). Thus, to quantify $pSer129^+$ inclusions, we proceeded with only the TSA technique. As always, the no-primary antibody group and PBS-infused mice did not show any of the characteristic threadlike and perinuclear inclusions, including in the infusion epicenter in the bulbar AON, but diffuse pSer129 immunoreactivity was observed within the rostral segments of the OB after PBS infusions (purposefully brightened for Fig. S3b), as reported (Killinger et al., 2023). We previously reported diffuse pSer129 label in the rostral OB as “background” (Mason et al., 2016), but it may be α-synuclein based on the Killinger et al. report. It is important to note that the latter type of immunolabel is *not* observed within the boundaries of the AON in PBS-infused mice—the region of our image analyses—even at long exposure settings [see Fig. 1C(a) of (Mason et al., 2016)]. Note that the OB, accumbens, cerebellum, and ventral mesencephalon were not included in our image analyses (see Supplemental Methods) in the present study, specifically to avoid diffuse pSer129 in these regions (Killinger et al., 2023).

Based on our finalized protocol for detecting pSer129, cryoprotected sections were washed with freshly filtered 10 mM PBS and incubated in permeabilization buffer (0.5% Triton X-100 in PBS) for 10 mins. Next, sections were incubated in peroxidase quenching buffer (0.3% hydrogen peroxide in PBS) for 15 mins, washed with PBS, and then incubated in blocking buffer (10% normal goat serum and 0.5% Triton X-100 in PBS) for 1 h at room temperature. Primary antibodies (Table S1) were prepared in a PBS solution containing 1.5% normal goat serum (005-000-121, Jackson ImmunoResearch, West Grove, PA) and 0.5% Triton X-100. Sections were incubated with primary antibodies overnight on a shaker at 4 °C. Unbound primary antibodies were washed off with PBS and sections were then

incubated in PBS containing 1.5% normal goat serum, 0.5% Triton X-100, and 5 μg/mL goat horseradish peroxidase-tagged secondary antibodies (Biotium) (Table S2) for 1 h at room temperature. Sections were washed with PBS and working solutions containing the *CF*-dye (92,172, Biotium) were prepared in Tyramide Amplification Buffer (Biotium), supplemented with fresh 0.0015% hydrogen peroxide immediately prior to use. Sections were incubated with the dye solution for 15 mins at room temperature and protected from light. Next, unbound dye molecules were washed off with three exchanges of PBS and sections were counterstained with Hoechst 33258 (bisBenzimide, 5 μg/mL; B1155, Sigma-Aldrich) for 20 min at room temperature, before mounting tissue sections on glass slides. Slides were then scanned on the Odyssey M Imager (LI-COR) at 5-μm resolution, as well as an Olympus VS200 slide scanner using a 20× objective. Representative images were captured on an Olympus microscope (Olympus IX73, B&B Microscopes) using a 4×, 20×, 40×, or 100× (oil) objective. Omission of primary antibodies led to the expected degree of loss of immunopositive signal. Control and experimental groups were always processed in parallel in the same solutions.

2.4. Statistical analyses

We did not conduct power analyses to determine group sizes in the present study. Mice were randomized for group allocation, with an *n* of 10 fibril-infused mice per group for behavior analyses, an *n* of 6–8 mice per group for flow cytometric analyses, and an *n* of 5 mice per group (randomized out of 10 PFF-infused mice) for the True AI/Deep Learning. All exclusion criteria are described in Methods and Figure Legends. Each statistical unit or *n* is illustrated as a colored dot in the bar graphs with means + SDs or in box plots with interquartile ranges. *In vitro* data from technical replicates (*i.e.*, cell culture plate wells) were averaged to obtain a single data point for each litter of rat pups (*i.e.,* each statistical unit is a different litter and, therefore, an independent biological replicate). Note that some *in vitro* data are shown as fold-change data to mitigate the impact of culture-to-culture variation, which reflects technical rather than biological variance, such as in plating densities and immunofluorescence staining intensities (*i.e.,* the 'batch' effect). *In vivo* data points are defined as individual animals in all graphs, except for sequentially extracted experiments, where three mouse samples were combined into one tube. Thus, the latter graphs show three dots or statistical units per group, but samples had been originally generated from nine mice per group.

For experiments with two groups, a two-tailed, unpaired *t*-test was performed if data displayed Gaussian distributions (per the Shapiro-Wilk test). For heteroscedastic data, Welch's *t*-test was performed. For normally distributed data with >2 groups, we performed a one, two, or three-way ANOVA followed by the Bonferroni *post hoc* test. Intervariable statistical interactions with biological sex are shown above respective graphs, as per guidelines on reporting sex differences (Garcia-Sifuentes and Maney, 2021). For non-normally distributed data, the Mann-Whitney *U* (2 groups) or Kruskal-Wallis (>2 groups) test was used. Other data that did not fit Gaussian distributions are presented as log-transformed or square-root values (always shown before *and* after transformation) to not violate the assumptions of parametric ANOVA testing.

For correlation testing, the two-tailed Pearson or Spearman analyses were employed, based on whether data were normally distributed or not, respectively. Statistical tests were performed using GraphPad Prism (Version 9) or IBM SPSS Statistics (Versions 23–26). Two-tailed alpha was set at 5%. As far as possible, data were gathered as well as analyzed by blinded observers (apart from immunoblotting data, where samples were loaded in an *a priori*, non-randomized order).

3. Results

3.1. Transient dietary PLX5622 induces sustained hyperactivity in fibril-injected aged mice

A large body of prior work suggests that dietary PLX5622 elicits microglia depletion and that withdrawal of PLX5622 elicits repopulation, including in aged mice (Barca et al., 2022; Casali et al., 2020; Dagher et al., 2015; Elmore et al., 2018; Henry et al., 2020; Rice et al., 2017; Spangenberg et al., 2019; Willis et al., 2020; Zhang et al., 2019), as we also confirmed here (Fig. S4). We performed flow cytometry (gating strategy in Fig. S4a–e) on the brains of 1) young male and female CD-1 mice fed PLX5622/control diet for two weeks, and 2) young male and female mice CD-1 fed control chow for an additional seven weeks (Fig. S4f; same timeline as in Fig. 1a). Due to resource constraints, we were unable to acquire additional aged, 18 month-old, sex-matched mice for these confirmatory experiments. First, we observed that >94% of $CD45^{+}CD11b^{+}F4/80^{+}$ monocytes in the brain were positive for microglia marker TMEM119 (Bennett et al., 2018; Bennett et al., 2016) (Fig. S4g). Biological sex or PLX5622 did not change the proportion of brain monocytes that were microglial (Fig. S4g). PLX5622 induced equivalent (~60%) microglial depletion in young male and female CD-1 mice (Fig. S4h–j), consistent with prior work in C57 mice (Johnson et al., 2023) and young male rats (Stoll et al., 2023).

Reversal to the control chow elicited the expected rebound in microglia numbers in both sexes, but to a slightly higher degree in females than males (Fig. S4h–j). Changes in numbers of $TMEM119^{+}$ cells (Fig. S4j) were not paralleled by robust changes in TMEM119 fluorescence intensity (Fig. S4k), suggesting that Fig. S4j does indeed reflect sex-biased changes in microglial cell *numbers* and not lability of the TMEM119 marker. The spleen had fewer $TMEM119^{+}$ cells compared to the brain, as expected (Fig. S4l). As PLX5622 withdrawal may also impact macrophages (*i.e.,* cells that are $CD45^{+}CD11b^{+}F4/80^{+}$, but $TMEM119^{-}$; Fig. S4m) we use the term microglia/macrophages where appropriate (also see Fig. S5h in (Zhang et al., 2019)). As a fraction of monocytes, microglia were the vast majority of the macrophage population (compare Y-axes of Fig. S4i and Fig. S4m). Thus, PLX5622 elicits microglia/macrophage depletion in CD-1 mice, and withdrawal of PLX5622 elicits microglia/macrophage repopulation, as expected.

We tested if transient PLX5622 exposure moderates the behavioral, biochemical, and histological consequences of α-synucleinopathy in our model of limbic Lewy body disease (Bhatia et al., 2021; Mason et al., 2016; Mason et al., 2019; Miner et al., 2022). In the PFF model, the density of Lewy-like pathology typically peaks ~8 weeks later in first-order afferents (Duffy et al., 2018b; Patterson et al., 2019; Paumier et al., 2015; Stoll and Sortwell, 2022). Hence, in our 18 month-old CD-1 mice that were being fed control/PLX5622

diets, we infused PFFs 8 weeks prior to sacrifice, or one week after initiating the pulse of PLX5622 (timeline in Fig. 1a). Within 7 days of PLX5622 delivery, a small loss in bodyweight was observed in aged male, but not aged females (Fig. S5). Loss of bodyweight in females exposed to PLX5622 was delayed and statistically significant only 14 days after initiation of the PLX5622 diet. In contrast, after PLX5622 withdrawal on day 14, mice of either sex did not lose additional bodyweight.

We originally intended to perform behavior testing *after* PLX5622 withdrawal. However, during the PLX5622 dosing regimen, some mice were quite skittish. Thus, the open field test was performed on all remaining mice still being administered PLX5622 (*i.e.*, immediately prior to withdrawing PLX5622; Fig. S6a–m) to quantify potential hyperactivity. No sex differences in the PFF-infused mice on the control diet (light gray bars in Fig. S6) were noted. However, females made more entries and spent more time in central squares of the open arena if fed PLX5622 (Fig. S6a–c). PLX5622-fed males made more entries into corner squares than control diet-fed males, and they spent more time in corner squares compared to PLX5622-fed females (Fig. S6d–e). If the amount of time spent in and number of entries made into the corner squares reflect anxiety, PFF-infused aged CD-1 males show greater anxiety-like behaviors when fed PLX5622 *vs.* control diet.

Both male and female mice had been more active on the PLX5622 diet in terms of distance traveled and speeds in the open field (Fig. S6f–g). Other measures of activity, such as maximum speed (Fig. S6h), time spent active (Fig. S6i), time spent mobile (Fig. S6j), time spent rearing (Fig. S6k), and number of rears (Fig. S6l) showed an increase with PLX5622 delivery in PFF-injected male but not female mice. A positive correlation (Fig. S6m) between the number of corner square entries and number of rears suggested that the increase in rearing episodes may be linked with anxiety-like phenotypes. Thus, biological sex modifies the impact of PLX5622 upon hyperactive/anxiety-like behaviors in PFF-injected mice, as noted with statistical interactions between the two independent variables in Fig. S6.

To determine if removal of PLX5622 from the diet reverses these deficits, we repeated the open field test on *all* mice after PLX5622 withdrawal (Fig. 1a,b). No statistically significant differences in number of entries into or time spent in central squares were noted (Fig. 1c–d). Despite PLX5622 withdrawal, males still made slightly more entries into corner squares than when fed the control diet (Fig. 1e). However, PLX5622-fed mice did not spend more time exploring corner squares than the control diet group (Fig. 1f), perhaps because they remained hyperactive, as evidenced by increases in locomotor measures (Fig. 1g–m). Thus, the hyperactivity observed in PFF-injected aged males in response to PLX5622 was not amended after PLX5622 withdrawal.

3.2. Transient dietary PLX5622 improves spatial reference memory in fibril-injected aged mice

Next, we tested if PFF infusions in the OB/AON elicit impairments on the forced alternation test for spatial reference memory, by comparing PFF-infused mice to PBS-infused mice in a Y-maze (Fig. 2a–g). PFF-infused mice made fewer entries into the novel arm, when this measure was expressed as a fraction of total arm entries—to control for hyperactivity

(Fig. 2a–c). PFF-infused mice also spent less time exploring the novel arm and made more entries into the familiar arms, compared to PBS-infused controls (Fig. 2d–f), indicative of impairments in reference memory in aged CD-1 mice infused with PFFs in the bulbar AON.

In comparison to mice on the control diet, transient PLX5622 increased novel arm entries in PFF-injected mice of both sexes (Fig. 2h). However, when the data were expressed as a fraction of *total* arm entries, the increase in novel arm entries was only statistically significant for female mice exposed to transient PLX5622 (Fig. 2i–j). The data in Fig. 2i confirm the open field findings, in that transient PLX5622 elicits a hyperactive phenotype in PFF-infused aged male mice. In contrast, female mice exposed transiently to PLX5622 made greater entries into the novel arm, fewer entries into familiar arms, spent greater time exploring the novel arm, and entered the novel arm earlier, compared to control diet-fed females (Fig. 2h–n).

Notably, the female-specific changes with PLX5622 may reflect worse reference memory in the control diet-fed aged females than males, as females on the control diet made more entries into and spent greater time exploring familiar arms (Fig. 2k, m), and they also made fewer entries into the novel arm and entered the novel arm later than control diet-fed males (Fig. 2j, n). Considered together with intervariable statistical interactions above respective graphs, these data suggest that reference memory deficits in PFF-injected aged females are surmountable with a dietary pulse of PLX5622.

No differences on the inverted grid test or on the spontaneous alternation test for spatial working memory were noted (not shown). PFF-injected aged mice on the control diet did not show statistically significant changes in marble burying behaviors (Fig. S7a–b). No differences in the latencies to contact exposed or buried food were noted (Fig. S7c–d). However, PFF-injected aged females on the control diet took longer than males to *eat* the pellet, which may reflect worse olfaction, lesser hunger, or lesser motivation/locomotion in aged females than males (Fig. S7e–f). Thus, transient PLX5622 improves spatial reference memory, particularly in PFF-injected aged female mice, but exerts little to no effect on the other behavior measures.

3.3. Transient dietary PLX5622 mitigates limbic α-synucleinopathy in fibril-injected aged mice

We evaluated the phosphorylation status of α-synuclein and its solubility in the nonionic detergent Triton X-100 after PFF infusions (Fig. 3, S8). Monomeric α-synuclein migrates at ~16–17 kDa through denaturing gels (Anderson et al., 2006; Sharon et al., 2001), as we also noted (Fig. 3a, S8a). PFF infusions raised insoluble α-synuclein levels in the OB/AON of aged mice, compared to PBS-infused mice, as expected (Fig. 3a–b, the same blots are shown in Fig. S8a). No differences were noted in the soluble fraction (data not shown). Bands of higher molecular mass were also visible and higher in PFF than PBS mice, with both pSer129 and pan α-synuclein antibodies (S8a and S8d–f), suggesting these are pathological forms of aggregated α-synuclein.

Both the pathological monomeric (~16–17 kDa) and higher molecular mass (>17 kDa) bands showed a reduction after transient PLX5622 delivery in male mice (Fig. 3b, S8d).

PLX5622 even elicited a slight reduction in the proportion of insoluble, monomeric α-synuclein that was phosphorylated at serine 129 (Fig. 3e), but similar changes were not observed for the higher-mass α-synuclein aggregates (Fig. 3h). The PLX5622-induced reductions in pSer129 and pan α-synuclein were largely attributed to aged males (Fig. 3b, Fig. S8d), although we caution that we were low on statistical power, because three murine OB/AON samples were collapsed into one for the ultracentrifugation step (see Supplemental Methods).

Next, we quantified the pSer129 fluorescent signal per unit area (Fig. 4a) in traces of the olfactory peduncle (defined by (Brunjes et al., 2011)) after performing a systematic evaluation of the tyramide signal amplification (TSA) technique (see Methods and Fig. S1–3). We did not observe a significant reduction in pSer129 signal after transient PLX5622 delivery (Fig. 4b). However, when data were sex-stratified, a reduction in pSer129 signal was noted in aged male mice fed PLX5622 transiently (Fig. 4c–d; heatmaps in Fig. 4e). The area data in Fig. 4d also reveal that olfactory peduncular regions were not undergoing shrinkage or atrophy after the PLX5622 pulse. The pSer129 signal in the olfactory peduncle was weakly inversely correlated with novel arm entries in the Y-maze—an effect largely attributable to males when linear regressions were stratified by sex (Fig. 4f–h).

To achieve higher resolution in calculations of α-synucleinopathic load, a blinded observer calculated the pSer129$^+$ load along the lateral limbic rhinencephalon (does not include the AON, OB, cerebellum, or other medial brain areas; see Methods) using Deep Learning (representative stitched images in Fig. 5k, Fig. S8g (high-magnification images of pSer129$^+$ inclusions), and S9 (high resolution image of Fig. 5k)). There was a sizable reduction in the numbers of pSer129$^+$ inclusions with transient PLX5622 (Fig. 5a), an effect again attributed to aged males (Fig. 5b). Aged PFF-infused females on the control diet harbored fewer inclusions compared to males (Fig. 5b), consistent with our prior work in younger CD-1 mice (Mason et al., 2019). There was no statistically significant reduction in the % total area occupied by the inclusions in the lateral rhinencephalon in PFF-injected aged mice after transient PLX5622 (Fig. 5c), until data were sex-stratified (Fig. 5d). Grayscale intensities of pSer129$^+$ structures were lower after transient PLX5622, and this effect was also attributable to males (Fig. 5e–f).

Thus, the impact of PLX5622 on α-synuclein$^+$ pathology in the bulbar AON was lower than on caudolateral regions of the rhinencephalon (compare data and effect sizes in Fig. 5 *versus* Figs. 3–4), and the effects were more prominent in aged males than females.

3.4 . Impact of transient PLX5622 on microglia/macrophages of the anterior olfactory nucleus

The Deep Learning tool was used to dissect morphologies of Iba1$^+$ microglia/macrophages at the infusion epicenter in the bulbar AON, including Iba1$^+$ cellular hydraulic indices, defined as indicators of microglial activation (George et al., 2019). No differences in Iba1$^+$ cell densities, Hoechst$^+$ cell densities, Hoechst$^+$ nuclear areas, or in total area occupied by Iba1$^+$ structures were noted, suggestive of successful repopulation of myeloid cells—at least in the AON—and no cell loss (Fig. S10a–e). However, the sizes (*i.e.,* areas) and perimeters of individual Iba1$^+$ cells, and their hydraulic radii (area / perimeter) were all lowered after

transient PLX5622 (Fig. S10f–h). Lowering of hydraulic indices indicates that the sizes of repopulated Iba1$^+$ cells in PLX5622-pulsed mice shrunk proportionately more than the perimeters, compared to control diet-fed mice. We also retrieved the shape factor (Fig. S10i–j), defined as a measure of roundedness (a value of 1.0 identifies a perfectly circular object). The shape factor was increased by 8.67% after transient PLX5622, suggesting that repopulated Iba1$^+$ cells were slightly more spherical (Fig. S10i–j). Thus, repopulated Iba1$^+$ cells may not have fully extended their processes or incorporated themselves into the surrounding matrices (also evident in low-power figures of Fig. S10a; see Discussion).

3.5. Transient PLX5622 exposure unexpectedly raised pSer129$^+$ inclusion sizes

The average sizes of the pSer129$^+$ inclusions were *greater* in PFF-infused aged mice after transient PLX5622 exposure, compared to aged mice fed the control diet (Fig. 5g–h). There was also a main statistical effect (two-tailed $p = 0.008$) of biological sex in the two-way ANOVA for Fig. 5h. In the pairwise comparisons with the Bonferroni *post hoc*, PFF-injected aged female mice on the control diet had larger inclusions compared to control diet-fed males (Fig. 5h). According to the Nearest Neighbor Distance function of the Deep Learning output, PLX5622 increased the linear distances between inclusions, but only in male mice (Fig. 5i–j).

To test the generalizability of our sex-specific findings to young microglial cells in a different species of outbred rodent, we leveraged an *in vitro* model of rat hippocampal microglia/neuron cocultures exposed to PFFs (Fig. 5l–o). We chose the hippocampus for region-specific microglia and neuron cocultures because primary hippocampal neurons have been used in well-standardized PFF *in vitro* work (Volpicelli-Daley et al., 2014) and we have validated this model in our hands (Bhatia et al., 2021; Miner et al., 2022). First, we show that our hippocampal microglia cultures responded to canonical stimuli, in that exposure to interleukin-4 (IL4) elicited an increase in anti-inflammatory CD206, whereas exposure to a cocktail of lipopolysaccharide and interferon-γ (LPS/IFNγ) elicited an increase in proinflammatory iNOS and CD16 (Fig. S11a–g). Acute treatment of primary hippocampal microglia with PFFs did not change the expression of these markers (Fig. S11e–g). However, primary hippocampal microglia were able to engulf PFFs (Fig. S11h–i). We then coadministered PFFs and microspheres (*i.e.*, fluorescent beads; Fig. S11j) and found that PFFs also increased the number of internalized microspheres (Fig. S11k–n). However, a successful reduction in actin or tubulin-dependent phagocytosis (with cytochalasin D or nocodazole, respectively; see Supplemental Methods) did not enhance or suppress the ability of PFFs to stimulate microglial engulfment of beads—because there was no statistical interaction between the two independent variables (PFF exposure *x* phagocytosis inhibition).

Next, we examined the sex-specific *functional* impact of postnatal primary microglia on α-synucleinopathy using sex-stratified glia/neuron hippocampal cocultures exposed to PFFs. Male, but not female microglia reduced the numbers of inclusions per Hoechst$^+$ cell in cocultures from the same sex. Although the effect size was slight (Fig. 5l–n), the male-specific effect in rat primary cultures was consistent with *in vivo* data in mice in Fig. 5b. No statistically significant differences in Hoechst$^+$ cell or NeuN$^+$ neuron viabilities were seen (Fig. S12a–c). Male, but not female microglia also slightly reduced inclusion

counts expressed as a fraction of NeuN$^+$ neurons, but only when fold-change data were analyzed (Fig. S12d–e), perhaps because the NeuN protein marker is labile, unlike the nuclear Hoechst stain (Bhatia et al., 2021). The total area occupied by inclusions also tended to be slightly lower in male cocultures (Fig. S12f–h), consistent with *in vivo* data in Fig. 5d.

Average sizes of the inclusions rose slightly when female microglia were cocultured with female neurons (Fig. 5o), also partially reproducing *in vivo* data in Fig. 5h. Thus, young or old microglia/macrophages moderate inclusion morphologies in the PFF model in a sex-biased manner, although the effect sizes may be higher in adulthood and *in vivo*.

3.6. A sex-biased association between spatial reference memory and inclusion morphologies

Finally, we tested the internal consistency of the pSer129$^+$ structural measurements made by the Neural Network with two-tailed correlation analyses in the lateral brain sections (Fig. 6 and Fig. S13). A tight positive link between inclusion numbers and pSer129 grayscale intensity or inclusion area fractions was confirmed (Fig. 6a–b). In contrast, inclusion sizes were *inversely* correlated with mean grayscale intensities and inclusion counts (Fig. 6c–d), suggesting that big inclusions housed less phosphorylated α-synuclein. Area fraction of inclusions was not associated with inclusion size but was positively correlated with mean grayscale intensity (Fig. S13a–b). Finally, the Nearest Neighbor Distance was inversely linked with inclusion counts, mean grayscale intensities, and area fractions, but not with inclusion sizes (Fig. S13e–h).

Although correlational links do not establish causality, we reasoned that an *absence* of correlations between inclusion measures and reference memory would refute the notion that limbic pSer129$^+$ structures influenced neurological outcomes. In our data, novel arm entries in the Y-maze were inversely associated with inclusion counts but positively correlated with inclusion sizes (Fig. 6e–f). Hence, larger (but fewer) inclusions are linked with superior reference memory. The negative links between novel arm entries and pSer129$^+$ inclusion counts or area fractions were only robust in males (Fig. 6i–l), whereas the positive link between novel arm entries and inclusion sizes was not truly sex-selective (Fig. S13c–d). The time spent exploring the novel arm (another measure of reference memory) was positively linked with inclusion sizes in females only (Fig. 6m–n). The nearest neighbor distance was also positively linked with novel arm entries in males (Fig. S13i–j).

In the Iba1-related data, the most robust correlations with pSer129$^+$ inclusion counts were formed by Iba1$^+$ area fraction (Fig. 6g). If the total area occupied by Iba1$^+$ cells can be viewed as one indicator of microglia/macrophage reactivity, then 1) higher inclusion counts may cause greater Iba1$^+$ cell reactivity, 2) higher Iba1$^+$ cell reactivity may elicit more inclusion numbers, or 3) the correlations are spurious. Notably, the bigger the pSer129$^+$ inclusions, the less area the Iba1$^+$ cells occupied in PFF-infused mice (Fig. 6h), revealing that big inclusions are associated with less occupation of brain volume by microglia/macrophages. Finally, the hydraulic radii (a measure of reactivity) of Iba1$^+$ cells were negatively linked with novel arm entries in males (Fig. 6o–p).

To summarize, we have used diverse approaches, including multiple behavior assays, True AI/Deep Learning to count α-synucleinopathic structures, and detergent-based fractionation to assess levels of insoluble α-synuclein in 18 month-old PFF-infused mice of both sexes. We also used sex-stratified limbic (hippocampus-specific) microglia/neuron cocultures to evaluate if and how young male *versus* female microglia affect inclusion sizes and counts. The evidence reported here suggests that male microglia tend to reduce inclusion counts whereas female microglia tend to expand inclusion sizes, and that high inclusion loads (counts and area fractions) in males are linked to worse spatial reference memory (Fig. 6i, k), but also that bigger inclusions in females may be indicative of better neurological outcomes (Fig. 6n).

4. Discussion

Dietary PLX5622 administration is recognized to elicit microglia depletion followed by repopulation upon withdrawal (Barca et al., 2022; Casali et al., 2020; Dagher et al., 2015; Elmore et al., 2018; Henry et al., 2020; Rice et al., 2017; Spangenberg et al., 2019; Willis et al., 2020; Zhang et al., 2019). Thus, we hypothesized that a 14-day pulse of PLX5622 would have therapeutic potential against early stage, limbic α-synucleinopathy. We report that PLX5622 withdrawal reduced levels of insoluble and phosphorylated α-synuclein, improved spatial reference memory, and mitigated microglia/macrophage reactivity in aged (18 month-old), outbred mice. However, behavior measures were not uniformly improved and sex-biased effects were noted.

4.1. Transient PLX5622 exposure modifies inclusion morphologies and neurological outcomes

A dietary pulse of PLX5622 reduced inclusion counts, pSer129$^+$ grayscale intensities, area fractions, and Triton X-insoluble α-synuclein in male mice only and raised the average sizes of inclusions in both sexes. Transient PLX5622 exposure also increased novel arm entries in PFF-infused aged mice, particularly in females. Higher numbers of pSer129$^+$ inclusions tended to 1) cluster together, 2) occupy greater swaths of the limbic rhinencephalon, 3) display more pSer129 (mean grayscale intensities), and 4) correlate with greater microglia/macrophage area fractions. Larger-sized inclusions, on the other hand, were linked to lower inclusion counts, pSer129 levels, and Iba1$^+$ area fractions. Although the biochemical effect sizes are modest compared to the AI/Deep Learning-driven histological analyses, we note that pSer129$^+$ structures are larger after transient PLX5622 exposure in both sexes, which may mask some of the biochemical effects.

In our hands, male microglia/macrophages tend to reduce limbic inclusion counts, whereas female microglia/macrophages tend to amplify limbic inclusion sizes. We also found that better memory was associated with fewer inclusions in males and larger-sized inclusions in females, but we add that the biological significance of a small *vs.* large inclusion is not yet understood. In humans, Lewy-related structures may undergo progressive compaction over time (Dale et al., 1992; Gomez-Tortosa et al., 2000) and in the PFF model, pSer129$^+$ immunoreactivity tends to fill more of the soma at early stages, and then evolves into smaller, compact structures (Duffy et al., 2018a; Miller et al., 2021; Osterberg et al.,

2015). Thus, in our model, larger inclusions upon PLX5622 withdrawal may reflect earlier/immature pathology and relative slowing of the disease in females, a hypothesis that could be tested with multiphoton *in vivo* imaging and adding more survival timepoints. Additional work is thus warranted to test if transient PLX5622 slows inclusion formation, accelerates degradation of aggregates, and/or changes dispersal of aggregates across the neuraxis.

In a mouse model of Alzheimer's disease, withdrawal of PLX5622 led to more compact amyloid plaques, suggesting that microglia protect the brain *via* β-amyloid plaque compaction (Casali et al., 2020). In contrast, we observe that withdrawal of PLX5622 amplifies the size of $pSer129^+$ structures, suggesting that the type (and perhaps intra *vs.* extracellular nature) of the aggregation complex is critical. We speculate that lowering the size of the protein aggregate "sink" in the cytosol may loosen spatial restrictions on the cellular pool of α-synuclein, increasing the probability of exit of unfettered α-synuclein aggregates out of the cell *via* exosomes or other means (Danzer et al., 2012; Grey et al., 2015; Howitt et al., 2021). An increase in cellular escape would provide dispersed aggregates with access to even more α-synuclein—the suspected substrate for prion-like seeding of additional inclusions—compared to when aggregates remain trapped within a bounded, small container (inclusion) in the original cell. Greater escape of α-synuclein from cellular boundaries may be associated with worse memory and smaller-sized inclusions for these reasons. Alternatively, there could be a complete uncoupling of Lewy-related inclusions from behavioral measures, and the correlations could all be coincidental.

We observed that a relatively brief exposure to dietary PLX5622 induced mild weight loss and anxiety-like behaviors in the PFF-infused aged males and hyperactive behaviors in mice of both sexes, although more locomotor changes were apparent in males. Hyperactive/anxiety-like measures were not reversed upon PLX5622 withdrawal. Prior work in an Alzheimer's disease model revealed that depletion of microglia may induce immediate-early genes and increase the probability of excitotoxicity (Johnson et al., 2023). Thus, in future work, the transcriptomes and cytokine profiles of PFF-infused males and females subjected to PLX5622 ought to be tested, particularly as repopulated microglia are derived from cells that survive CSF1R inhibition (Huang et al., 2018). In addition, the bioavailability of PLX5622 should also be examined in the PFF model, as was recently completed in an Alzheimer's disease model (Johnson et al., 2023).

Under baseline conditions, PFF infusions impaired spatial reference memory, with aged females exhibiting worse performance than male counterparts. After transient PLX5622 exposure, females displayed more dynamic changes in Y-maze cognitive outcomes, perhaps due to greater room for cognitive improvement than males. In contrast, transient PLX5622 did not rescue other behavior deficits, perhaps because some brain areas may be targeted to a greater extent by CSF1R inhibitors. For example, the hippocampus shows higher expression of *Csf1r*, compared to other areas such as the striatum, globus pallidus, posterior cortex, cerebellum, frontal cortex, nigra, and thalamus (DropViz database by (Saunders et al., 2018)). Furthermore, recent reports suggest that microglia first reappear in the subventricular zone after repopulation and then migrate to other brain regions along white matter tracts (Hohsfield et al., 2021). Hence, region-dependent changes in response to PLX5622 are worth examining in the PFF model in the future.

4.2. Hippocampal microglia reduce pSer129^{+} inclusions in cocultured hippocampal neurons

Our *in vivo* observations were partially recapitulated *in vitro* when sex-stratified primary microglia were added to primary hippocampal neurons of the same sex as the glia. To our knowledge, sex differences in the abilities of young, primary microglia to regulate α-synuclein pathology have not been reported, although our data are consistent with sex-specific phenotypes in cultured microglia (Villa et al., 2018). Furthermore, these sex differences were evident within days after birth, reinforcing the idea that they are at least partly genetically determined, perhaps by sex-specific chromosomes such as *Sry* (Kashimada and Koopman, 2010; Lee et al., 2019).

4.3. Use of CSF1R inhibitors in models of aging, α-synucleinopathies, and/or parkinsonism

Many groups have shown that microglia are long-lived, have slow turnover, and may be transporters of α-synuclein, and proposed that phagocytosis is impaired in Lewy body disease (Bido et al., 2021; Fuger et al., 2017; Guo et al., 2020; Reu et al., 2017; Salman et al., 1999; Xia et al., 2019). Thus, a sizable body of work supported testing whether microglia depletion reduces α-synucleinopathy. In this context, prior work showed that CSF1R inhibitors are protective in the PFF (Guo et al., 2020), rotenone (Jing et al., 2021; Zhang et al., 2021a), and 6-hydroxydopamine (Oh et al., 2020) models. Others, however, showed that CSF1R inhibitors increase pathology, worsen disease outcomes, and induce neurotoxicity (George et al., 2019; Pereira et al., 2023; Yang et al., 2018), and some suggest that CSF1R inhibition exerts no beneficial effects in PFF-infused young male rats (Stoll et al., 2023).

On the surface, the aforementioned reports of microglia/macrophage *depletion* in preclinical models of Lewy body-related disease lack consistency. Furthermore, only young animals of one sex were tested, or the sex was left unmentioned (George et al., 2019; Guo et al., 2020; Jing et al., 2021; Oh et al., 2020; Stoll et al., 2023; Yang et al., 2018; Zhang et al., 2021a). Although studies of microglia/macrophage *repopulation* after depletion are fewer, they have shown more consistently beneficial results in models of aging, acute brain injury, Alzheimer's disease, intracerebral hemorrhage, inflammation, stroke, and parkinsonism (Barca et al., 2022; Coleman Jr. et al., 2020; Elmore et al., 2018; Henry et al., 2020; Johnson et al., 2023; Li et al., 2021; Li et al., 2022; Rice et al., 2017; Rowe et al., 2022; Willis et al., 2020).

With aging, microglia show lower phagocytosis, less protrusion of processes, reduced motility, greater lipofuscin, more mitochondrial damage, and higher inflammatory cytokine expression (Angelova and Brown, 2019; Spittau, 2017). Thus, resetting the aging microglial phenotype by the short-term delivery of CSF1R inhibitors has begun to receive attention. Transient delivery of CSF1R inhibitors may be more likely to succeed in the clinic, as the sustained use of CSF1R inhibitors may be toxic (see below).

In our hands, male and female CD-1 mice showed equivalent (~60%) loss of microglia. This is modest, compared to ~90% loss of microglia in seminal studies (Liu et al., 2019; Rosin

et al., 2018; Spangenberg et al., 2019). However, our findings are more consistent with recent work in sex-stratified mice (Johnson et al., 2023) and male rats (Stoll et al., 2023). Sex differences in microglia/macrophage depletion have been reported in rats, with greater depletion in females (Sharon et al., 2022). Although we did not find sex differences in microglia/macrophage depletion, repopulation of TMEM119^{+} microglia in the whole brain was slightly higher in young female mice compared to males. However, the more reactive and labile marker, Iba1, did not reveal sex differences in repopulated microglia/macrophages in the AON of PFF-infused aged mice (in our hands, the TMEM119 antibodies we tried did not work well outside of flow cytometry). We relied on Iba1 for Fig. S10, as Iba1 provides better visualization of microglial morphologies, compared to TMEM119 (Gonzalez Ibanez et al., 2019). In sum, some of the sex-specific effects could reflect differences in microglial depletion/repopulation, brain region of interest, or depend on the microglial marker used.

Recent work reveals that long-term delivery (without withdrawal) of the CSF1R inhibitor PLX3397 for six months after PFF infusions in the striata of young male rats increases somal size of remaining microglia/macrophages in the substantia nigra, without robustly affecting nigral inclusions or dopaminergic neurodegeneration (Stoll et al., 2023). The True AI/Deep Learning did not separate measurements of Iba1^{+} cell processes *versus* somata, but we note that after a 14-day pulse of PLX5622 in our aging mice, repopulated Iba1^{+} cells in the AON were smaller as well as rounder. This is consistent with prior work showing that transient PLX5622 exposure lowers Iba1^{+} coverage and thins Iba1^{+} processes in aged mice, making the repopulated microglia/macrophages in aged mice closer to young mice in morphology (see Fig. 2 of (Elmore et al., 2018)). In the latter report, somal size was examined in young mice only (Fig. S1 of (Elmore et al., 2018)) and showed no long-term changes after transient PLX5622 exposure.

Newly born microglia after PLX5622 withdrawal may be immature initially and only acquire maturity over time (Zhan et al., 2019). We observe a slight increase in sphericity of repopulated microglia/macrophages, perhaps because they are less mature and have not yet fully extended their processes into the surrounding matrix. The reduction in Iba1^{+} cellular size and subtle increase in sphericity was not associated with evidence of higher microglia/macrophage reactivity in our model. Some studies in stroke models suggest that sphericity may be associated with microglial reactivity (Benakis et al., 2022), whereas others argue that spherical microglia are “resting” cells (Nakagawa et al., 2022). The repopulated, slightly more spherical microglia in PFF-infused mice could also be more phagocytic, as microglia assume a more spherical shape during engulfment (Kettenmann et al., 2011; Lai and Todd, 2006; Lai and Todd, 2008; Lyu et al., 2021). Furthermore, microglia can use their branches to build a spherical enclosure around the site of injury, perhaps to build a barrier and/or remove toxic signals and debris (Brawek et al., 2021). Thus, the evidence suggests that polymorphisms in microglia structure facilitate a diversity of functional effects based on the disease/injury/aging context.

4.4. Strengths and limitations of using CSF1R inhibitors to target microglia/macrophages

Recent reports suggest that high amounts of CSF1R inhibitors exert off-target effects (Lei et al., 2020), including on other brain cells and on members of the adaptive immune

system (Lei et al., 2021; Liu et al., 2019). This may have contributed to our results, as non-microglial immune cells also regulate pSer129 pathology (Earls et al., 2020; George et al., 2021). The non-specificity of PLX5622 and PLX3397 is attributable to CSF1R expression on multiple cell types, including macrophages, Langerhans cells (skin), osteoclasts, oocytes, decidual cells, trophoblastic cells, Paneth cells (intestine), and myoblasts (Li et al., 2006; Mun et al., 2020). Accordingly, CSF1R inhibition at embryogenesis elicits craniofacial and dental abnormalities in rodent pups (Rosin et al., 2018), and CSF1R knockouts not only show loss of microglia/macrophages, but also ~50% loss of oligodendroglia (Erblich et al., 2011). The latter mice show enlarged ventricles, a disintegrated OB, atrophy of brain tissue, and impaired olfaction and reproduction (Erblich et al., 2011; Li et al., 2006). On the other hand, we did not see a reduction in $Hoechst^{+}$ nuclei counts or evidence of nuclear shrinkage with a 14-day PLX5622 exposure. It has been suggested that PLX5622 exerts off-target effects on oligodendroglia only if given for 21 d or longer (Liu et al., 2019). In contrast, the less selective CSF1R inhibitor PLX3397 elicits earlier loss of oligodendrocyte progenitor cells (Liu et al., 2019). It is worth noting that all microglia depletion methods show off-target effects and are associated with caveats (Giuliani et al., 2005; Lund et al., 2017). As PLX5622 is being tested in clinical trials as an anti-inflammatory agent for rheumatoid arthritis (NCT01329991), it could be repurposed for other conditions, but exposure to CSF1R inhibitors may have to be limited to brief periods to be effective.

A key caveat of our work is that we cannot cleanly attribute effects to repopulation of microglia/macrophage during the PLX5622 withdrawal period vis-à-vis microglia/macrophage depletion during oral intake of PLX5622 (at the time of PFF infusions). As chronic depletion by itself is not effective in the PFF model (Stoll et al., 2023), we speculate that the present findings are more likely to be attributed to repopulation rather than depopulation. We also caution that resetting microglia/macrophages as a therapeutic intervention against neurological disease may interfere with unexpected homeostatic roles of microglia even in late-stage Lewy body disease. Additional limitations of our work include the use of young mice for the initial flow cytometric analyses of microglial depopulation and repopulation, and our current lack of knowledge on the biological relevance of small *vs.* large-sized inclusions. Further scrutiny of off-target effects of PLX5622, including the loss of body mass and increase in hyperactive behaviors, also seem essential prior to use of CSF1R inhibitors in the elderly and frail.

5. Conclusions

Stimulating microglia/macrophage turnover with CSF1R blockade is associated with fewer memory deficits and lower inclusion pathology, consistent with the view that microglia and macrophages sculpt neural circuitry, assist in synaptoplasticity, and impact memory (Chung et al., 2015; Cornell et al., 2022; Schafer and Stevens, 2015). It is difficult to explain why males benefitted more from transient PLX5622 exposure in terms of histological and biochemical outcomes whereas females benefitted more in behavioral changes. Perhaps a reduction in inclusion counts *and* a concomitant increase in inclusion size are crucial, and only males showed both changes. Our work also suggests that the conflicting literature on toxic *vs.* beneficial roles of Lewy bodies may be explained by distinct sequelae of larger inclusion sizes *vs.* more inclusion numbers.

Ultimately, we will need to fully understand the biochemical and biophysical properties of smaller *vs.* larger sized inclusions, and their functional impact on extracellular dispersal, seeding, and behavioral neurotoxicity. Further studies on oligomeric *versus* fibrillar properties and the membrane association properties of aggregates of different sizes are warranted. We also that hope our findings stimulate further work to test if transient PLX5622-fed mice display 1) better engulfment of protein aggregates from the extracellular space, 2) higher release of trophic factors and lower release of inflammatory cytokines into the interstitial and cerebrospinal fluid compartments, and 3) more efferocytosis of dysfunctional neurons. In our limbic-centered model, we do not observe extensive neurodegeneration (Mason et al., 2019), but future work could also examine the impact of targeting microglia with CSF1R inhibition in aggregation *vs.* degenerative phases of the disease (Stoll and Sortwell, 2022).

Supplementary Material

Refer to Web version on PubMed Central for supplementary material.

Acknowledgments

The authors are grateful to Yashika Kamte for technical support, Sherri Nichol and Christie Manspeaker for administrative support, and to Rachel Barr and Ashley Yuhouse for animal care.

Funding

National Institutes for Health grants R15NS130532-01 (RKL), 1R03NS088395-01A1 (RKL), 1R15NS093539-01 (RKL), 1R21NS107960-01 (RKL), and R35GM131732 (JLB). TNB's 2019–2020 stipend was generously funded by the University of Pittsburgh's *Center for Protein Conformational Diseases*. The authors are also grateful to the Graduate School of Pharmaceutical Sciences for their support of Duquesne graduate students. Jun Chen is a recipient of the VA Senior Research Career Scientist Award.

Data availability

Supporting data can be accessed by contacting Rehana Leak at leakr@duq.edu

Abbreviations:

AON	Anterior olfactory nucleus
CSF1R	Colony stimulating factor 1 receptor
DLB	Dementia with Lewy bodies
DMEM	Dulbecco's Modified Eagle Medium
HBBS	Hank's Balanced Salt Solution
IL4	Interleukin 4
LPS/IFNγ	Lipopolysaccharide/interferon-gamma
OB	Olfactory bulb
PD	Parkinson's disease

PBS	Phosphate buffered saline
pSer129	Phosphorylated alpha-synuclein at Ser129
PFFs	Preformed fibrils
TSA	Tyramide Signal Amplification

References

Aldinger KA, Sokoloff G, Rosenberg DM, Palmer AA, Millen KJ, 2009. Genetic variation and population substructure in outbred CD-1 mice: implications for genome-wide association studies. PLoS One 4, e4729. [PubMed: 19266100]

Anderson JP, Walker DE, Goldstein JM, de Laat R, Banducci K, Caccavello RJ, Barbour R, Huang J, Kling K, Lee M, Diep L, Keim PS, Shen X, Chataway T, Schlossmacher MG, Seubert P, Schenk D, Sinha S, Gai WP, Chilcote TJ, 2006. Phosphorylation of Ser-129 is the dominant pathological modification of alpha-synuclein in familial and sporadic Lewy body disease. J. Biol. Chem. 281, 29739–29752. [PubMed: 16847063]

Angelova DM, Brown DR, 2019. Microglia and the aging brain: are senescent microglia the key to neurodegeneration? J. Neurochem. 151, 676–688. [PubMed: 31478208]

Attems J, Walker L, Jellinger KA, 2014. Olfactory bulb involvement in neurodegenerative diseases. Acta Neuropathol. 127, 459–475. [PubMed: 24554308]

Attems J, Toledo JB, Walker L, Gelpi E, Gentleman S, Halliday G, Hortobagyi T, Jellinger K, Kovacs GG, Lee EB, Love S, McAleese KE, Nelson PT, Neumann M, Parkkinen L, Polvikoski T, Sikorska B, Smith C, Grinberg LT, Thal DR, Trojanowski JQ, McKeith IG, 2021. Neuropathological consensus criteria for the evaluation of Lewy pathology in post-mortem brains: a multi-Centre study. Acta Neuropathol. 141, 159–172. [PubMed: 33399945]

Bachstetter AD, Van Eldik LJ, Schmitt FA, Neltner JH, Ighodaro ET, Webster SJ, Patel E, Abner EL, Kryscio RJ, Nelson PT, 2015. Disease-related microglia heterogeneity in the hippocampus of Alzheimer's disease, dementia with Lewy bodies, and hippocampal sclerosis of aging. Acta Neuropathol. Commun. 3, 32. [PubMed: 26001591]

Barca C, Kiliaan AJ, Wachsmuth L, Foray C, Hermann S, Faber C, Schafers M, Wiesmann M, Zinnhardt B, Jacobs AH, 2022. Short-term colony-stimulating factor 1 receptor inhibition-induced repopulation after stroke assessed by longitudinal (18)F-DPA-714 PET imaging. J. Nucl. Med. 63, 1408–1414. [PubMed: 35115368]

Barth M, Bacioglu M, Schwarz N, Novotny R, Brandes J, Welzer M, Mazzitelli S, Hasler LM, Schweighauser M, Wuttke TV, Kronenberg-Versteeg D, Fog K, Ambjorn M, Alik A, Melki R, Kahle PJ, Shimshek DR, Koch H, Jucker M, Tanriover G, 2021. Microglial inclusions and neurofilament light chain release follow neuronal alpha-synuclein lesions in long-term brain slice cultures. Mol. Neurodegener. 16, 54. [PubMed: 34380535]

Beach TG, Adler CH, Lue L, Sue LI, Bachalakuri J, Henry-Watson J, Sasse J, Boyer S, Shirohi S, Brooks R, Eschbacher J, White CL 3rd, Akiyama H, Caviness J, Shill HA, Connor DJ, Sabbagh MN, Walker DG, Arizona Parkinson's Disease C, 2009a. Unified staging system for Lewy body disorders: correlation with nigrostriatal degeneration, cognitive impairment and motor dysfunction. Acta Neuropathol. 117, 613–634. [PubMed: 19399512]

Beach TG, White CL 3rd, Hladik CL, Sabbagh MN, Connor DJ, Shill HA, Sue LI, Sasse J, Bachalakuri J, Henry-Watson J, Akiyama H, Adler CH, Arizona Parkinson's Disease C, 2009b. Olfactory bulb alpha-synucleinopathy has high specificity and sensitivity for Lewy body disorders. Acta Neuropathol. 117, 169–174. [PubMed: 18982334]

Benakis C, Simats A, Tritschler S, Heindl S, Besson-Girard S, Llovera G, Pinkham K, Kolz A, Ricci A, Theis FJ, Bittner S, Gokce O, Peters A, Liesz A, 2022. T cells modulate the microglial response to brain ischemia. Elife 11.

Bennett ML, Bennett FC, Liddelow SA, Ajami B, Zamanian JL, Fernhoff NB, Mulinyawe SB, Bohlen CJ, Adil A, Tucker A, Weissman IL, Chang EF, Li G, Grant GA, Hayden Gephart MG, Barres BA,

2016. New tools for studying microglia in the mouse and human CNS. Proc. Natl. Acad. Sci. U. S. A. 113, E1738–E1746. [PubMed: 26884166]

Bennett FC, Bennett ML, Yaqoob F, Mulinyawe SB, Grant GA, Hayden Gephart M, Plowey ED, Barres BA, 2018. A combination of ontogeny and CNS environment establishes microglial identity. Neuron 98 (1170–1183), e8.

Bhatia TN, Clark RN, Needham PG, Miner KM, Jamenis AS, Eckhoff EA, Abraham N, Hu X, Wipf P, Luk KC, Brodsky JL, Leak RK, 2021. Heat shock protein 70 as a sex-skewed regulator of alpha-synucleinopathy. Neurotherapeutics 18, 2541–2564. [PubMed: 34528172]

Bido S, Muggeo S, Massimino L, Marzi MJ, Giannelli SG, Melacini E, Nannoni M, Gambare D, Bellini E, Ordazzo G, Rossi G, Maffezzini C, Iannelli A, Luoni M, Bacigaluppi M, Gregori S, Nicassio F, Broccoli V, 2021. Microglia-specific overexpression of alpha-synuclein leads to severe dopaminergic neurodegeneration by phagocytic exhaustion and oxidative toxicity. Nat. Commun. 12, 6237. [PubMed: 34716339]

Braak H, Del Tredici K, Rub U, de Vos RA, Jansen Steur EN, Braak E, 2003. Staging of brain pathology related to sporadic Parkinson's disease. Neurobiol. Aging 24, 197–211. [PubMed: 12498954]

Brawek B, Skok M, Garaschuk O, 2021. Changing functional signatures of microglia along the Axis of brain aging. Int. J. Mol. Sci. 22.

Brunjes PC, Kay RB, Arrivillaga JP, 2011. The mouse olfactory peduncle. J. Comp. Neurol. 519, 2870–2886. [PubMed: 21618219]

Casali BT, MacPherson KP, Reed-Geaghan EG, Landreth GE, 2020. Microglia depletion rapidly and reversibly alters amyloid pathology by modification of plaque compaction and morphologies. Neurobiol. Dis. 142, 104956. [PubMed: 32479996]

Choi I, Zhang Y, Seegobin SP, Pruvost M, Wang Q, Purtell K, Zhang B, Yue Z, 2020. Microglia clear neuron-released alpha-synuclein via selective autophagy and prevent neurodegeneration. Nat. Commun. 11, 1386. [PubMed: 32170061]

Chung WS, Welsh CA, Barres BA, Stevens B, 2015. Do glia drive synaptic and cognitive impairment in disease? Nat. Neurosci. 18, 1539–1545. [PubMed: 26505565]

Coleman LG Jr., Zou J, Crews FT, 2020. Microglial depletion and repopulation in brain slice culture normalizes sensitized proinflammatory signaling. J. Neuroinflammation 17, 27. [PubMed: 31954398]

Cornell J, Salinas S, Huang HY, Zhou M, 2022. Microglia regulation of synaptic plasticity and learning and memory. Neural Regen. Res. 17, 705–716. [PubMed: 34472455]

Dagher NN, Najafi AR, Kayala KM, Elmore MR, White TE, Medeiros R, West BL, Green KN, 2015. Colony-stimulating factor 1 receptor inhibition prevents microglial plaque association and improves cognition in 3xTg-AD mice. J. Neuroinflammation 12, 139. [PubMed: 26232154]

Dai YB, Tan XJ, Wu WF, Warner M, Gustafsson JA, 2012. Liver X receptor beta protects dopaminergic neurons in a mouse model of Parkinson disease. Proc. Natl. Acad. Sci. U. S. A. 109, 13112–13117. [PubMed: 22826221]

Dale GE, Probst A, Luthert P, Martin J, Anderton BH, Leigh PN, 1992. Relationships between Lewy bodies and pale bodies in Parkinson's disease. Acta Neuropathol. 83, 525–529. [PubMed: 1320323]

Danzer KM, Kranich LR, Ruf WP, Cagsal-Getkin O, Winslow AR, Zhu L, Vanderburg CR, McLean PJ, 2012. Exosomal cell-to-cell transmission of alpha synuclein oligomers. Mol. Neurodegener. 7, 42. [PubMed: 22920859]

Delic V, Chandra S, Abdelmotilib H, Maltbie T, Wang S, Kem D, Scott HJ, Underwood RN, Liu Z, Volpicelli-Daley LA, West AB, 2018. Sensitivity and specificity of phospho-Ser129 alpha-synuclein monoclonal antibodies. J. Comp. Neurol. 526, 1978–1990. [PubMed: 29888794]

Duffy MF, Collier TJ, Patterson JR, Kemp CJ, Fischer DL, Stoll AC, Sortwell CE, 2018a. Quality over quantity: advantages of using alpha-synuclein preformed fibril triggered synucleinopathy to model idiopathic Parkinson's disease. Front. Neurosci. 12, 621. [PubMed: 30233303]

Duffy MF, Collier TJ, Patterson JR, Kemp CJ, Luk KC, Tansey MG, Paumier KL, Kanaan NM, Fischer DL, Polinski NK, Barth OL, Howe JW, Vaikath NN, Majbour NK, El-Agnaf OMA,

Sortwell CE, 2018b. Lewy body-like alpha-synuclein inclusions trigger reactive microgliosis prior to nigral degeneration. J. Neuroinflammation 15, 129. [PubMed: 29716614]

Earls RH, Menees KB, Chung J, Gutekunst CA, Lee HJ, Hazim MG, Rada B, Wood LB, Lee JK, 2020. NK cells clear alpha-synuclein and the depletion of NK cells exacerbates synuclein pathology in a mouse model of alpha-synucleinopathy. Proc. Natl. Acad. Sci. U. S. A. 117, 1762–1771. [PubMed: 31900358]

Elmore MR, Najafi AR, Koike MA, Dagher NN, Spangenberg EE, Rice RA, Kitazawa M, Matusow B, Nguyen H, West BL, Green KN, 2014. Colony-stimulating factor 1 receptor signaling is necessary for microglia viability, unmasking a microglia progenitor cell in the adult brain. Neuron 82, 380–397. [PubMed: 24742461]

Elmore MRP, Hohsfield LA, Kramar EA, Soreq L, Lee RJ, Pham ST, Najafi AR, Spangenberg EE, Wood MA, West BL, Green KN, 2018. Replacement of microglia in the aged brain reverses cognitive, synaptic, and neuronal deficits in mice. Aging Cell 17, e12832. [PubMed: 30276955]

Erblich B, Zhu L, Etgen AM, Dobrenis K, Pollard JW, 2011. Absence of colony stimulation factor-1 receptor results in loss of microglia, disrupted brain development and olfactory deficits. PLoS One 6, e26317. [PubMed: 22046273]

Flores-Cuadrado A, Saiz-Sanchez D, Mohedano-Moriano A, Lamas-Cenjor E, Leon-Olmo V, Martinez-Marcos A, Ubeda-Banon I, 2021. Astrogliosis and sexually dimorphic neurodegeneration and microgliosis in the olfactory bulb in Parkinson's disease. NPJ. Parkinsons Dis. 7, 11. [PubMed: 33479244]

Fuger P, Hefendehl JK, Veeraraghavalu K, Wendeln AC, Schlosser C, Obermuller U, Wegenast-Braun BM, Neher JJ, Martus P, Kohsaka S, Thunemann M, Feil R, Sisodia SS, Skodras A, Jucker M, 2017. Microglia turnover with aging and in an Alzheimer's model via long-term in vivo single-cell imaging. Nat. Neurosci. 20, 1371–1376. [PubMed: 28846081]

Garcia-Sifuentes Y, Maney DL, 2021. Reporting and misreporting of sex differences in the biological sciences. Elife 10.

George S, Rey NL, Tyson T, Esquibel C, Meyerdirk L, Schulz E, Pierce S, Burmeister AR, Madaj Z, Steiner JA, Escobar Galvis ML, Brundin L, Brundin P, 2019. Microglia affect alpha-synuclein cell-to-cell transfer in a mouse model of Parkinson's disease. Mol. Neurodegener. 14, 34. [PubMed: 31419995]

George S, Tyson T, Rey NL, Sheridan R, Peelaerts W, Becker K, Schulz E, Meyerdirk L, Burmeister AR, von Linstow CU, Steiner JA, Galvis MLE, Ma J, Pospisilik JA, Labrie V, Brundin L, Brundin P, 2021. T cells limit accumulation of aggregate pathology following Intrastriatal injection of alpha-synuclein fibrils. J. Parkinsons Dis. 11, 585–603. [PubMed: 33579871]

Giuliani F, Hader W, Yong VW, 2005. Minocycline attenuates T cell and microglia activity to impair cytokine production in T cell-microglia interaction. J. Leukoc. Biol. 78, 135–143. [PubMed: 15817702]

Gomez-Tortosa E, Newell K, Irizarry MC, Sanders JL, Hyman BT, 2000. Alpha-Synuclein immunoreactivity in dementia with Lewy bodies: morphological staging and comparison with ubiquitin immunostaining. Acta Neuropathol. 99, 352–357. [PubMed: 10787032]

Gonzalez Ibanez F, Picard K, Bordeleau M, Sharma K, Bisht K, Tremblay ME, 2019. Immunofluorescence staining using IBA1 and TMEM119 for microglial density, morphology and peripheral myeloid cell infiltration analysis in mouse brain. J. Vis. Exp. 152, e60510.

Grey M, Dunning CJ, Gaspar R, Grey C, Brundin P, Sparr E, Linse S, 2015. Acceleration of alpha-synuclein aggregation by exosomes. J. Biol. Chem. 290, 2969–2982. [PubMed: 25425650]

Guneykaya D, Ivanov A, Hernandez DP, Haage V, Wojtas B, Meyer N, Maricos M, Jordan P, Buonfiglioli A, Gielniewski B, Ochocka N, Comert C, Friedrich C, Artiles LS, Kaminska B, Mertins P, Beule D, Kettenmann H, Wolf SA, 2018. Transcriptional and translational differences of microglia from male and female brains. Cell Rep. 24 (2773–2783), e6.

Guo M, Wang J, Zhao Y, Feng Y, Han S, Dong Q, Cui M, Tieu K, 2020. Microglial exosomes facilitate alpha-synuclein transmission in Parkinson's disease. Brain 143, 1476–1497. [PubMed: 32355963]

Haenseler W, Zambon F, Lee H, Vowles J, Rinaldi F, Duggal G, Houlden H, Gwinn K, Wray S, Luk KC, Wade-Martins R, James WS, Cowley SA, 2017. Excess alpha-synuclein compromises phagocytosis in iPSC-derived macrophages. Sci. Rep. 7, 9003. [PubMed: 28827786]

Halliday GM, Stevens CH, 2011. Glia: initiators and progressors of pathology in Parkinson's disease. Mov. Disord. 26, 6–17. [PubMed: 21322014]

Han J, Fan Y, Zhou K, Blomgren K, Harris RA, 2021. Uncovering sex differences of rodent microglia. J. Neuroinflammation 18, 74. [PubMed: 33731174]

Hanamsagar R, Bilbo SD, 2016. Sex differences in neurodevelopmental and neurodegenerative disorders: focus on microglial function and neuroinflammation during development. J. Steroid Biochem. Mol. Biol. 160, 127–133. [PubMed: 26435451]

Hanamsagar R, Alter MD, Block CS, Sullivan H, Bolton JL, Bilbo SD, 2017. Generation of a microglial developmental index in mice and in humans reveals a sex difference in maturation and immune reactivity. Glia 65, 1504–1520. [PubMed: 28618077]

Harms AS, Delic V, Thome AD, Bryant N, Liu Z, Chandra S, Jurkuvenaite A, West AB, 2017. Alpha-Synuclein fibrils recruit peripheral immune cells in the rat brain prior to neurodegeneration. Acta Neuropathol. Commun. 5, 85. [PubMed: 29162163]

Harms AS, Ferreira SA, Romero-Ramos M, 2021. Periphery and brain, innate and adaptive immunity in Parkinson's disease. Acta Neuropathol. 141, 527–545. [PubMed: 33555429]

Henry RJ, Ritzel RM, Barrett JP, Doran SJ, Jiao Y, Leach JB, Szeto GL, Wu J, Stoica BA, Faden AI, Loane DJ, 2020. Microglial depletion with CSF1R inhibitor during chronic phase of experimental traumatic brain injury reduces neurodegeneration and neurological deficits. J. Neurosci. 40, 2960–2974. [PubMed: 32094203]

Hohsfield LA, Najafi AR, Ghorbanian Y, Soni N, Crapser J, Figueroa Velez DX, Jiang S, Royer SE, Kim SJ, Henningfield CM, Anderson A, Gandhi SP, Mortazavi A, Inlay MA, Green KN, 2021. Subventricular zone/white matter microglia reconstitute the empty adult microglial niche in a dynamic wave. Elife 10.

Hong S, Scherer DC, Singh N, Mendiratta SK, Serizawa I, Koezuka Y, Van Kaer L, 1999. Lipid antigen presentation in the immune system: lessons learned from CD1d knockout mice. Immunol. Rev. 169, 31–44. [PubMed: 10450506]

Howitt J, Low LH, Bouman M, Yang J, Gordon S, Hill A, Tan S-S, 2021. Exosomal transmission of α-synuclein initiates Parkinson's disease-like pathology. bioRxiv. 10.1101/2021.05.10.443522.

Hsieh LS, Wen JH, Miyares L, Lombroso PJ, Bordey A, 2017. Outbred CD1 mice are as suitable as inbred C57BL/6J mice in performing social tasks. Neurosci. Lett. 637, 142–147. [PubMed: 27871995]

Huang Y, Xu Z, Xiong S, Sun F, Qin G, Hu G, Wang J, Zhao L, Liang YX, Wu T, Lu Z, Humayun MS, So KF, Pan Y, Li N, Yuan TF, Rao Y, Peng B, 2018. Repopulated microglia are solely derived from the proliferation of residual microglia after acute depletion. Nat. Neurosci. 21, 530–540. [PubMed: 29472620]

Jing L, Hou L, Zhang D, Li S, Ruan Z, Zhang X, Hong JS, Wang Q, 2021. Microglial activation mediates noradrenergic locus coeruleus neurodegeneration via complement receptor 3 in a rotenone-induced Parkinson's disease mouse model. J. Inflamm. Res. 14, 1341–1356. [PubMed: 33859489]

Johnson NR, Yuan P, Castillo E, Lopez TP, Yue W, Bond A, Rivera BM, Sullivan MC, Hirouchi M, Giles K, Aoyagi A, Condello C, 2023. CSF1R inhibitors induce a sex-specific resilient microglial phenotype and functional rescue in a tauopathy mouse model. Nat. Commun. 14, 118. [PubMed: 36624100]

Kashimada K, Koopman P, 2010. Sry: the master switch in mammalian sex determination. Development 137, 3921–3930. [PubMed: 21062860]

Kettenmann H, Hanisch UK, Noda M, Verkhratsky A, 2011. Physiology of microglia. Physiol. Rev. 91, 461–553. [PubMed: 21527731]

Killinger BA, Mercado G, Choi S, Tittle T, Chu Y, Brundin P, Kordower JH, 2023. Distribution of phosphorylated alpha-synuclein in non-diseased brain implicates olfactory bulb mitral cells in synucleinopathy pathogenesis. NPJ. Parkinsons Dis. 9, 43. [PubMed: 36966145]

Klusa VZ, Isajevs S, Svirina D, Pupure J, Beitnere U, Rumaks J, Svirskis S, Jansone B, Dzirkale Z, Muceniece R, Kalvinsh I, Vinters HV, 2010. Neuroprotective properties of mildronate, a small molecule, in a rat model of Parkinson's disease. Int. J. Mol. Sci. 11, 4465–4487. [PubMed: 21151450]

Kodama L, Gan L, 2019. Do microglial sex differences contribute to sex differences in neurodegenerative diseases? Trends Mol. Med. 25, 741–749. [PubMed: 31171460]

Lai AY, Todd KG, 2006. Hypoxia-activated microglial mediators of neuronal survival are differentially regulated by tetracyclines. Glia 53, 809–816. [PubMed: 16541436]

Lai AY, Todd KG, 2008. Differential regulation of trophic and proinflammatory microglial effectors is dependent on severity of neuronal injury. Glia 56, 259–270. [PubMed: 18069670]

Lashuel HA, Mahul-Mellier AL, Novello S, Hegde RN, Jasiqi Y, Altay MF, Donzelli S, DeGuire SM, Burai R, Magalhaes P, Chiki A, Ricci J, Boussouf M, Sadek A, Stoops E, Iseli C, Guex N, 2022. Revisiting the specificity and ability of phospho-S129 antibodies to capture alpha-synuclein biochemical and pathological diversity. NPJ. Parkinsons Dis. 8, 136. [PubMed: 36266318]

Lee J, Pinares-Garcia P, Loke H, Ham S, Vilain E, Harley VR, 2019. Sex-specific neuroprotection by inhibition of the Y-chromosome gene, SRY, in experimental Parkinson's disease. Proc. Natl. Acad. Sci. U. S. A. 116, 16577–16582. [PubMed: 31371505]

Lei F, Cui N, Zhou C, Chodosh J, Vavvas DG, Paschalis EI, 2020. CSF1R inhibition by a small-molecule inhibitor is not microglia specific; affecting hematopoiesis and the function of macrophages. Proc. Natl. Acad. Sci. U. S. A. 117, 23336–23338. [PubMed: 32900927]

Lei F, Cui N, Zhou C, Chodosh J, Vavvas DG, Paschalis EI, 2021. CSF1R inhibition by small molecule affects T-helper cell differentiation independently of microglia depletion. 10.1101/2021.12.21.473532.

Lenz KM, McCarthy MM, 2015. A starring role for microglia in brain sex differences. Neuroscientist 21, 306–321. [PubMed: 24871624]

Lenz KM, Nugent BM, Haliyur R, McCarthy MM, 2013. Microglia are essential to masculinization of brain and behavior. J. Neurosci. 33, 2761–2772. [PubMed: 23407936]

Li J, Chen K, Zhu L, Pollard JW, 2006. Conditional deletion of the colony stimulating factor-1 receptor (c-fms proto-oncogene) in mice. Genesis 44, 328–335. [PubMed: 16823860]

Li Q, Shen C, Liu Z, Ma Y, Wang J, Dong H, Zhang X, Wang Z, Yu M, Ci L, Sun R, Shen R, Fei J, Huang F, 2021. Partial depletion and repopulation of microglia have different effects in the acute MPTP mouse model of Parkinson's disease. Cell Prolif. 54, e13094. [PubMed: 34312932]

Li X, Gao X, Zhang W, Liu M, Han Z, Li M, Lei P, Liu Q, 2022. Microglial replacement in the aged brain restricts neuroinflammation following intracerebral hemorrhage. Cell Death Dis. 13, 33. [PubMed: 35013119]

Liu Y, Given KS, Dickson EL, Owens GP, Macklin WB, Bennett JL, 2019. Concentration-dependent effects of CSF1R inhibitors on oligodendrocyte progenitor cells ex vivo and in vivo. Exp. Neurol. 318, 32–41. [PubMed: 31029597]

Luk KC, Song C, O'Brien P, Stieber A, Branch JR, Brunden KR, Trojanowski JQ, Lee VM, 2009. Exogenous alpha-synuclein fibrils seed the formation of Lewy body-like intracellular inclusions in cultured cells. Proc. Natl. Acad. Sci. U. S. A. 106, 20051–20056. [PubMed: 19892735]

Luk KC, Kehm V, Carroll J, Zhang B, O'Brien P, Trojanowski JQ, Lee VM, 2012. Pathological alpha-synuclein transmission initiates Parkinson-like neurodegeneration in nontransgenic mice. Science 338, 949–953. [PubMed: 23161999]

Lund H, Pieber M, Harris RA, 2017. Lessons learned about neurodegeneration from microglia and monocyte depletion studies. Front. Aging Neurosci. 9, 234. [PubMed: 28804456]

Lyu J, Xie D, Bhatia TN, Leak RK, Hu X, Jiang X, 2021. Microglial/macrophage polarization and function in brain injury and repair after stroke. CNS Neurosci. Ther. 27, 515–527. [PubMed: 33650313]

Mason DM, Nouraei N, Pant DB, Miner KM, Hutchison DF, Luk KC, Stolz JF, Leak RK, 2016. Transmission of alpha-synucleinopathy from olfactory structures deep into the temporal lobe. Mol. Neurodegener. 11, 49. [PubMed: 27363576]

Mason DM, Wang Y, Bhatia TN, Miner KM, Trbojevic SA, Stolz JF, Luk KC, Leak RK, 2019. The center of olfactory bulb-seeded alpha-synucleinopathy is the limbic system and the ensuing pathology is higher in male than in female mice. Brain Pathol. 29, 741–770. [PubMed: 30854742]

McGeer PL, McGeer EG, Itagaki S, Mizukawa K, 1987. Anatomy and pathology of the basal ganglia. Can. J. Neurol. Sci. 14, 363–372.

McGeer PL, Itagaki S, Boyes BE, McGeer EG, 1988. Reactive microglia are positive for HLA-DR in the substantia nigra of Parkinson's and Alzheimer's disease brains. Neurology 38, 1285–1291. [PubMed: 3399080]

Miller KM, Patterson JR, Kochmanski J, Kemp CJ, Stoll AC, Onyekpe CU, Cole-Strauss A, Steece-Collier K, Howe JW, Luk KC, Sortwell CE, 2021. Striatal afferent BDNF is disrupted by synucleinopathy and partially restored by STN DBS. J. Neurosci. 41, 2039–2052. [PubMed: 33472823]

Miner KM, Jamenis AS, Bhatia TN, Clark RN, Rajasundaram D, Sauvaigo S, Mason DM, Posimo JM, Abraham N, DeMarco BA, Hu X, Stetler RA, Chen J, Sanders LH, Luk KC, Leak RK, 2022. alpha-synucleinopathy exerts sex-dimorphic effects on the multipurpose DNA repair/redox protein APE1 in mice and humans. Prog. Neurobiol. 216, 102307. [PubMed: 35710046]

Mun SH, Park PSU, Park-Min KH, 2020. The M-CSF receptor in osteoclasts and beyond. Exp. Mol. Med. 52, 1239–1254. [PubMed: 32801364]

Nakagawa Y, Lee J, Liu Y, Abbasi S, Hong T, Cabral H, Uchida S, Ebara M, 2022. Microglial immunoregulation by apoptotic cellular membrane mimetic polymeric particles. ACS Macro Lett. 11, 270–275. [PubMed: 35574780]

Nelson LH, Saulsbery AI, Lenz KM, 2019. Small cells with big implications: microglia and sex differences in brain development, plasticity and behavioral health. Prog. Neurobiol. 176, 103–119. [PubMed: 30193820]

Nouraei N, Mason DM, Miner KM, Carcella MA, Bhatia TN, Dumm BK, Soni D, Johnson DA, Luk KC, Leak RK, 2018. Critical appraisal of pathology transmission in the alpha-synuclein fibril model of Lewy body disorders. Exp. Neurol. 299, 172–196. [PubMed: 29056362]

Oh SJ, Ahn H, Jung KH, Han SJ, Nam KR, Kang KJ, Park JA, Lee KC, Lee YJ, Choi JY, 2020. Evaluation of the neuroprotective effect of microglial depletion by CSF-1R inhibition in a Parkinson's animal model. Mol. Imaging Biol. 22, 1031–1042. [PubMed: 32086763]

Olanow CW, Savolainen M, Chu Y, Halliday GM, Kordower JH, 2019. Temporal evolution of microglia and alpha-synuclein accumulation following foetal grafting in Parkinson's disease. Brain 142, 1690–1700. [PubMed: 31056668]

Osborne BF, Turano A, Schwarz JM, 2018. Sex differences in the neuroimmune system. Curr. Opin. Behav. Sci. 23, 118–123. [PubMed: 30014014]

Osterberg VR, Spinelli KJ, Weston LJ, Luk KC, Woltjer RL, Unni VK, 2015. Progressive aggregation of alpha-synuclein and selective degeneration of lewy inclusion-bearing neurons in a mouse model of parkinsonism. Cell Rep. 10, 1252–1260. [PubMed: 25732816]

Park JY, Paik SR, Jou I, Park SM, 2008. Microglial phagocytosis is enhanced by monomeric alpha-synuclein, not aggregated alpha-synuclein: implications for Parkinson's disease. Glia 56, 1215–1223. [PubMed: 18449945]

Patterson JR, Duffy MF, Kemp CJ, Howe JW, Collier TJ, Stoll AC, Miller KM, Patel P, Levine N, Moore DJ, Luk KC, Fleming SM, Kanaan NM, Paumier KL, El-Agnaf OMA, Sortwell CE, 2019. Time course and magnitude of alpha-synuclein inclusion formation and nigrostriatal degeneration in the rat model of synucleinopathy triggered by intrastriatal alpha-synuclein preformed fibrils. Neurobiol. Dis. 130, 104525. [PubMed: 31276792]

Paumier KL, Luk KC, Manfredsson FP, Kanaan NM, Lipton JW, Collier TJ, Steece-Collier K, Kemp CJ, Celano S, Schulz E, Sandoval IM, Fleming S, Dirr E, Polinski NK, Trojanowski JQ, Lee VM, Sortwell CE, 2015. Intrastriatal injection of pre-formed mouse alpha-synuclein fibrils into rats triggers alpha-synuclein pathology and bilateral nigrostriatal degeneration. Neurobiol. Dis. 82, 185–199. [PubMed: 26093169]

Pearce RK, Hawkes CH, Daniel SE, 1995. The anterior olfactory nucleus in Parkinson's disease. Movement Dis. Off. J. Movement Disorder Soc. 10, 283–287.

Pereira CPM, Francis-Oliveira J, Singulani MP, Ferreira AFF, Britto LRG, 2023. Microglial depletion exacerbates motor impairment and dopaminergic neuron loss in a 6-OHDA model of Parkinson's disease. J. Neuroimmunol. 375, 578019. [PubMed: 36681049]

Reu P, Khosravi A, Bernard S, Mold JE, Salehpour M, Alkass K, Perl S, Tisdale J, Possnert G, Druid H, Frisen J, 2017. The lifespan and turnover of microglia in the human brain. Cell Rep. 20, 779–784. [PubMed: 28746864]

Rey NL, Steiner JA, Maroof N, Luk KC, Madaj Z, Trojanowski JQ, Lee VM, Brundin P, 2016. Widespread transneuronal propagation of alpha-synucleinopathy triggered in olfactory bulb mimics prodromal Parkinson's disease. J. Exp. Med. 213, 1759–1778. [PubMed: 27503075]

Rey NL, George S, Steiner JA, Madaj Z, Luk KC, Trojanowski JQ, Lee VM, Brundin P, 2018. Spread of aggregates after olfactory bulb injection of alpha-synuclein fibrils is associated with early neuronal loss and is reduced long term. Acta Neuropathol. 135, 65–83. [PubMed: 29209768]

Rice RA, Pham J, Lee RJ, Najafi AR, West BL, Green KN, 2017. Microglial repopulation resolves inflammation and promotes brain recovery after injury. Glia 65, 931–944. [PubMed: 28251674]

Rosin JM, Vora SR, Kurrasch DM, 2018. Depletion of embryonic microglia using the CSF1R inhibitor PLX5622 has adverse sex-specific effects on mice, including accelerated weight gain, hyperactivity and anxiolytic-like behaviour. Brain Behav. Immun. 73, 682–697. [PubMed: 30056204]

Rowe RK, Green TRF, Giordano KR, Ortiz JB, Murphy SM, Opp MR, 2022. Microglia are necessary to regulate sleep after an immune challenge. Biology (Basel) 11.

Salman H, Bergman M, Djaldetti R, Bessler H, Djaldetti M, 1999. Decreased phagocytic function in patients with Parkinson's disease. Biomed. Pharmacother. 53, 146–148. [PubMed: 10349503]

Saunders A, Macosko EZ, Wysoker A, Goldman M, Krienen FM, de Rivera H, Bien E, Baum M, Bortolin L, Wang S, Goeva A, Nemesh J, Kamitaki N, Brumbaugh S, Kulp D, McCarroll SA, 2018. Molecular diversity and specializations among the cells of the adult mouse brain. Cell 174 (1015–1030), e16.

Schafer DP, Stevens B, 2015. Microglia function in central nervous system development and plasticity. Cold Spring Harb. Perspect. Biol. 7, a020545. [PubMed: 26187728]

Scheiblich H, Dansokho C, Mercan D, Schmidt SV, Bousset L, Wischhof L, Eikens F, Odainic A, Spitzer J, Griep A, Schwartz S, Bano D, Latz E, Melki R, Heneka MT, 2021. Microglia jointly degrade fibrillar alpha-synuclein cargo by distribution through tunneling nanotubes. Cell 184 (5089–5106), e21.

Sharon R, Goldberg MS, Bar-Josef I, Betensky RA, Shen J, Selkoe DJ, 2001. Alpha-Synuclein occurs in lipid-rich high molecular weight complexes, binds fatty acids, and shows homology to the fatty acid-binding proteins. Proc. Natl. Acad. Sci. U. S. A. 98, 9110–9115. [PubMed: 11481478]

Sharon A, Erez H, Spira ME, 2022. Significant sex differences in the efficacy of the CSF1R inhibitor-PLX5622 on rat brain microglia elimination. Pharmaceuticals 15, 569. [PubMed: 35631395]

Spangenberg E, Severson PL, Hohsfield LA, Crapser J, Zhang J, Burton EA, Zhang Y, Spevak W, Lin J, Phan NY, Habets G, Rymar A, Tsang G, Walters J, Nespi M, Singh P, Broome S, Ibrahim P, Zhang C, Bollag G, West BL, Green KN, 2019. Sustained microglial depletion with CSF1R inhibitor impairs parenchymal plaque development in an Alzheimer's disease model. Nat. Commun. 10, 3758. [PubMed: 31434879]

Spittau B, 2017. Aging microglia-phenotypes, functions and implications for age-related neurodegenerative diseases. Front. Aging Neurosci. 9, 194. [PubMed: 28659790]

Stevenson TJ, Murray HC, Turner C, Faull RLM, Dieriks BV, Curtis MA, 2020. alpha-synuclein inclusions are abundant in non-neuronal cells in the anterior olfactory nucleus of the Parkinson's disease olfactory bulb. Sci. Rep. 10, 6682. [PubMed: 32317654]

Stoll AC, Sortwell CE, 2022. Leveraging the preformed fibril model to distinguish between alpha-synuclein inclusion- and nigrostriatal degeneration-associated immunogenicity. Neurobiol. Dis. 171, 105804. [PubMed: 35764290]

Stoll AC, Kemp CJ, Patterson JR, Kubik M, Kuhn N, Benskey MJ, Duffy MF, Luk KC, Sortwell C, 2023. Microglial depletion does not impact alpha-synuclein aggregation or nigrostriatal degeneration in the rat preformed fibril model. PREPRINT (Version 1) available at Research Square. 10.21203/rs.3.rs-2890683/v1.

Streit WJ, Xue QS, 2016. Microglia in dementia with Lewy bodies. Brain Behav. Immun. 55, 191–201. [PubMed: 26518296]

Streit WJ, Sammons NW, Kuhns AJ, Sparks DL, 2004. Dystrophic microglia in the aging human brain. Glia 45, 208–212. [PubMed: 14730714]

Swarnkar S, Goswami P, Kamat PK, Patro IK, Singh S, Nath C, 2013. Rotenone-induced neurotoxicity in rat brain areas: a study on neuronal and neuronal supportive cells. Neuroscience 230, 172–183. [PubMed: 23098804]

Tanriover G, Bacioglu M, Schweighauser M, Mahler J, Wegenast-Braun BM, Skodras A, Obermuller U, Barth M, Kronenberg-Versteeg D, Nilsson KPR, Shimshek DR, Kahle PJ, Eisele YS, Jucker M, 2020. Prominent microglial inclusions in transgenic mouse models of alpha-synucleinopathy that are distinct from neuronal lesions. Acta Neuropathol. Commun. 8, 133. [PubMed: 32787922]

Thakur P, Breger LS, Lundblad M, Wan OW, Mattsson B, Luk KC, Lee VMY, Trojanowski JQ, Bjorklund A, 2017. Modeling Parkinson's disease pathology by combination of fibril seeds and alpha-synuclein overexpression in the rat brain. Proc. Natl. Acad. Sci. U. S. A. 114, E8284–E8293. [PubMed: 28900002]

VanRyzin JW, Marquardt AE, Argue KJ, Vecchiarelli HA, Ashton SE, Arambula SE, Hill MN, McCarthy MM, 2019. Microglial phagocytosis of newborn cells is induced by endocannabinoids and sculpts sex differences in juvenile rat social play. Neuron 102 (435–449), e6.

Verma DK, Seo BA, Ghosh A, Ma SX, Hernandez-Quijada K, Andersen JK, Ko HS, Kim YH, 2021. Alpha-synuclein preformed fibrils induce cellular senescence in Parkinson's disease models. Cells 10.

Villa A, Gelosa P, Castiglioni L, Cimino M, Rizzi N, Pepe G, Lolli F, Marcello E, Sironi L, Vegeto E, Maggi A, 2018. Sex-specific features of microglia from adult mice. Cell Rep. 23, 3501–3511. [PubMed: 29924994]

Villa A, Della Torre S, Maggi A, 2019. Sexual differentiation of microglia. Front. Neuroendocrinol. 52, 156–164. [PubMed: 30481522]

Volpicelli-Daley LA, Luk KC, Patel TP, Tanik SA, Riddle DM, Stieber A, Meaney DF, Trojanowski JQ, Lee VM, 2011. Exogenous alpha-synuclein fibrils induce Lewy body pathology leading to synaptic dysfunction and neuron death. Neuron 72, 57–71. [PubMed: 21982369]

Volpicelli-Daley LA, Luk KC, Lee VM, 2014. Addition of exogenous alpha-synuclein preformed fibrils to primary neuronal cultures to seed recruitment of endogenous alpha-synuclein to Lewy body and Lewy neurite-like aggregates. Nat. Protoc. 9, 2135–2146. [PubMed: 25122523]

Weiss F, Labrador-Garrido A, Dzamko N, Halliday G, 2022. Immune responses in the Parkinson's disease brain. Neurobiol. Dis. 168, 105700. [PubMed: 35314321]

Willis EF, MacDonald KPA, Nguyen QH, Garrido AL, Gillespie ER, Harley SBR, Bartlett PF, Schroder WA, Yates AG, Anthony DC, Rose-John S, Ruitenberg MJ, Vukovic J, 2020. Repopulating microglia promote brain repair in an IL-6-dependent manner. Cell 180 (833–846), e16.

Wolf A, Bauer B, Abner EL, Ashkenazy-Frolinger T, Hartz AM, 2016. A comprehensive behavioral test battery to assess learning and memory in 129S6/Tg2576 mice. PLoS One 11, e0147733. [PubMed: 26808326]

Xia Y, Zhang G, Han C, Ma K, Guo X, Wan F, Kou L, Yin S, Liu L, Huang J, Xiong N, Wang T, 2019. Microglia as modulators of exosomal alpha-synuclein transmission. Cell Death Dis. 10, 174. [PubMed: 30787269]

Yang X, Ren H, Wood K, Li M, Qiu S, Shi FD, Ma C, Liu Q, 2018. Depletion of microglia augments the dopaminergic neurotoxicity of MPTP. FASEB J. 32, 3336–3345. [PubMed: 29401614]

Yanguas-Casás N, 2020. Physiological sex differences in microglia and their relevance in neurological disorders. Neuroimmunol. Neuroinflamm. 7, 13–22.

Zhan L, Krabbe G, Du F, Jones I, Reichert MC, Telpoukhovskaia M, Kodama L, Wang C, Cho SH, Sayed F, Li Y, Le D, Zhou Y, Shen Y, West B, Gan L, 2019. Proximal recolonization by self-renewing microglia re-establishes microglial homeostasis in the adult mouse brain. PLoS Biol. 17, e3000134. [PubMed: 30735499]

Zhang Q, Zhu W, Xu F, Dai X, Shi L, Cai W, Mu H, Hitchens TK, Foley LM, Liu X, Yu F, Chen J, Shi Y, Leak RK, Gao Y, Chen J, Hu X, 2019. The interleukin-4/PPARgamma signaling axis promotes oligodendrocyte differentiation and remyelination after brain injury. PLoS Biol. 17, e3000330. [PubMed: 31226122]

Zhang D, Li S, Hou L, Jing L, Ruan Z, Peng B, Zhang X, Hong JS, Zhao J, Wang Q, 2021a. Microglial activation contributes to cognitive impairments in rotenone-induced mouse Parkinson's disease model. J. Neuroinflammation 18, 4. [PubMed: 33402167]

Zhang W, Fan X, Fan Z, Wu B, Wang M, Duan W, Song B, 2021b. Acute exposure to paraquat affects the phenotypic differentiation of substantia nigra microglia in rats. Environ. Sci. Pollut. Res. Int. 29, 21339–21347. [PubMed: 34761315]

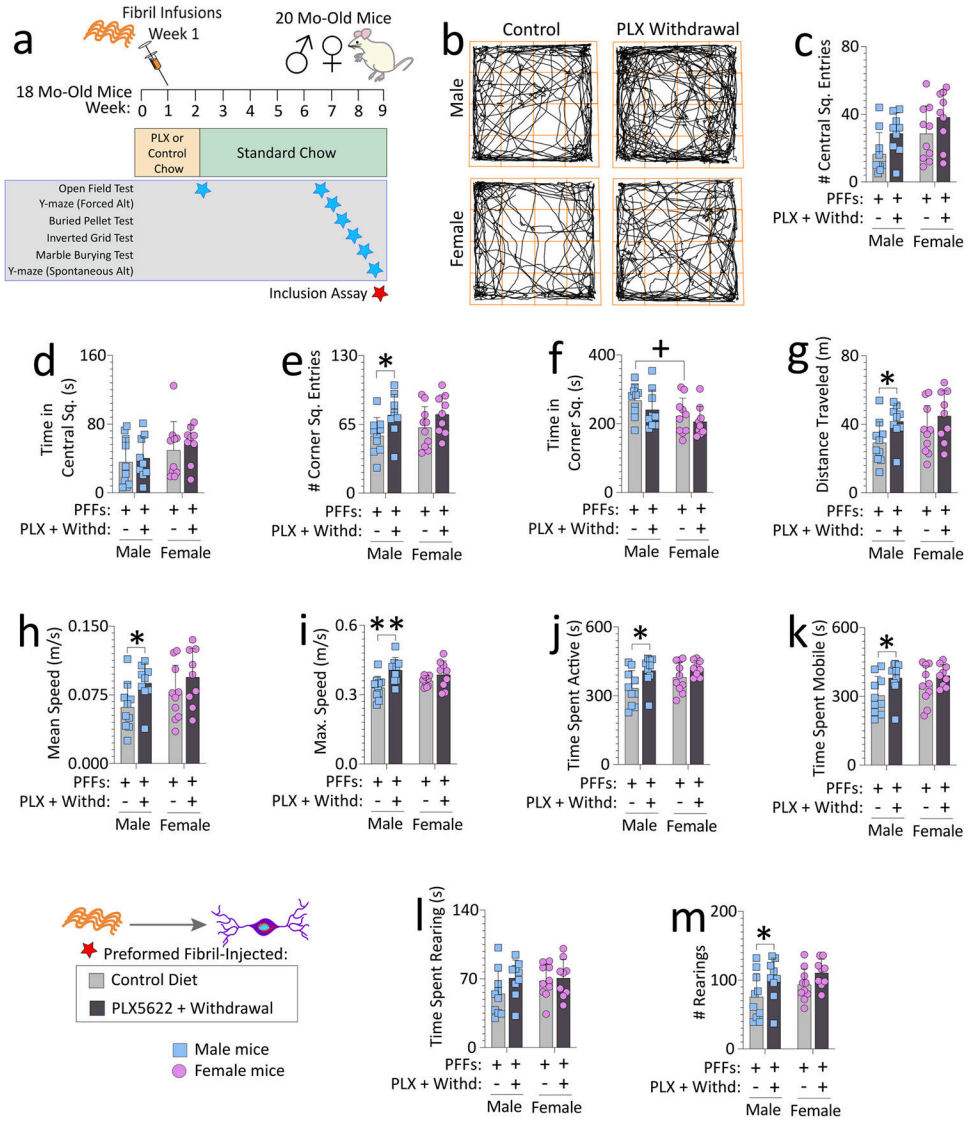

Fig. 1. Impact of transient exposure to the CSF1R antagonist PLX5622 (2-weeks "ON" and 7-weeks "OFF") on open-field behaviors in preformed fibril-injected aged mice.

Aged, outbred CD-1 mice of both sexes were fed special chow with or without the CSF1R inhibitor, PLX5622, for two weeks, and then fed standard rodent chow for an additional 7 weeks. Preformed fibrils (PFFs; 5 μg in 1 μL) were injected into the bulbar anterior olfactory nucleus seven days after initiation of the PLX5622 diet (**a**). For evidence of PLX5622-driven depletion and repopulation of microglia/macrophages, see Figs. S4 and S10a. Mice were tested in an open-field arena after PLX5622 withdrawal (timeline in **a**; data for the open-field test *during* PLX5622 delivery are in Fig. S6). (**b**) Representative trackplots from ANY-maze. Numbers of central square entries (**c**) and the time spent in central squares (**d**) are shown. Numbers of corner square entries (**e**), time spent in corner squares (**f**), distance traveled (**g**), mean speeds (**h**), maximum speeds (**i**), time spent active (such as grooming) (**j**), time spent mobile (moving) (**k**), time spent rearing (**l**), and numbers of rears (**m**) are shown. Out of $n = 40$ PFF-infused mice, two mice were sacrificed early due to dermatitis and an abdominal abscess and thus excluded from the open field test (see

Methods). Each mouse is illustrated as a colored dot on bar graphs with group means + SDs. $*p \leq 0.0500$, $**p \leq 0.0100$ for control diet *vs.* transient dietary PLX5622; $+p \leq 0.0500$ for male *vs.* female two-way ANOVA/Bonferroni. All testing was two-tailed.

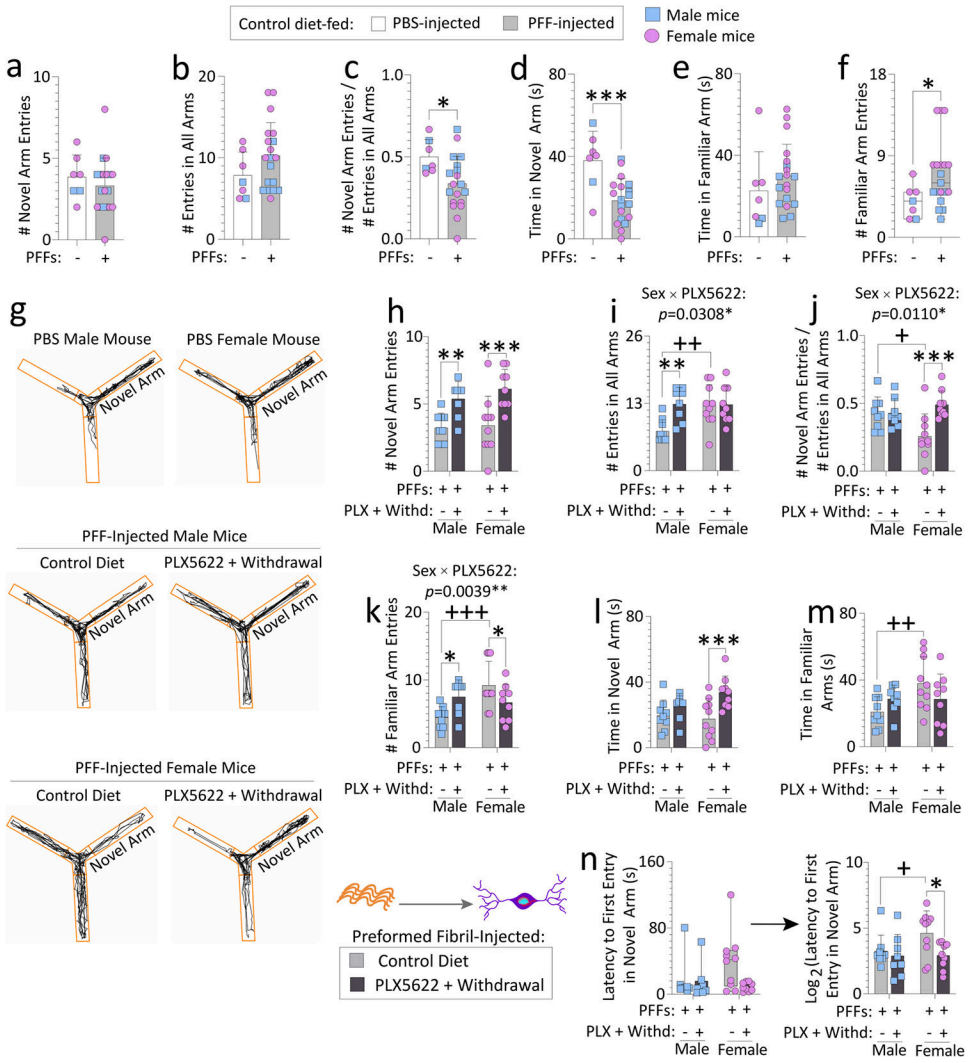

Fig. 2. Transient exposure to PLX5622 (2-weeks "ON" and 7-weeks "OFF") improves spatial reference memory in preformed fibril-injected aged female mice.

Aged, outbred CD-1 mice of both sexes were fed special chow with or without the CSF1R inhibitor, PLX5622, for two weeks, and then fed standard rodent chow for an additional 7 weeks (timeline in Fig. 1a). Preformed fibrils (PFFs; 5 μg in 1 μL) were injected into the bulbar anterior olfactory nucleus seven days after initiation of the PLX5622 diet. PFF-injected mice were tested on a Y-maze for spatial reference memory after PLX5622 was withdrawn from the diet (timeline in Fig. 1a). PBS-injected aged mice from each sex (total $n = 7$ across both sexes; remaining $n = 2$ PBS-infused aged mice had to be euthanized early due to sickness, see Methods) were included as controls to determine if PFF-infusions *per se* elicit loss of spatial reference memory (**a-f**). Numbers of novel arm entries are shown, expressed alone or as a fraction of total number of entries in all arms (**a-c**), to control for differences in activity. Time spent exploring the novel and familiar arms (**d-e**) and numbers of familiar arm entries (**f**) are shown, for the PBS *versus* PFF-infused aged mice. For control or transient PLX5622-diet fed, PFF-injected aged mice, numbers of novel arm entries (expressed alone in **h** or as a fraction of total number of entries in all arms in **i-j**),

numbers of familiar arm entries (**k**), time spent exploring the novel arm (**l**), time spent exploring the familiar arms (**m**), and latencies to first entry in the novel arm (**n**) are shown. In **g** are representative ANY-maze trackplots. Out of the $n = 40$ PFF-infused mice, two mice were sacrificed early due to dermatitis and an abdominal abscess and were excluded from the Y-maze test (see Methods). Mice that made less than three arm entries during the first minute of the second Y-maze trial were also excluded (see SI Methods and (Wolf et al., 2016)). Data in **n** were non-Gaussian per the Shapiro-Wilk test and log-transformed (arrow) to assess statistical interactions between the two independent variables. Intervariable statistical interactions are shown above respective graphs. Each mouse is illustrated as a colored dot on bar graphs with group means + SDs or on box plots with interquartile ranges. $*p \leq 0.0500$, $***p \leq 0.0010$ for PBS *vs.* PFFs; Mann-Whitney U (boxplot in **f**) or the unpaired t-test (**a-e**). $*p \leq 0.0500$, $**p \leq 0.0100$, $***p \leq 0.0010$ for control diet *vs.* transient dietary PLX5622; $+p \leq 0.0500$, $++p \leq 0.0100$, $+++p \leq 0.0010$ for male *vs.* female; Kruskal-Wallis (left panel of **n**) or two-way ANOVA/Bonferroni for **h-m** and right panel of **n**. All testing was two-tailed.

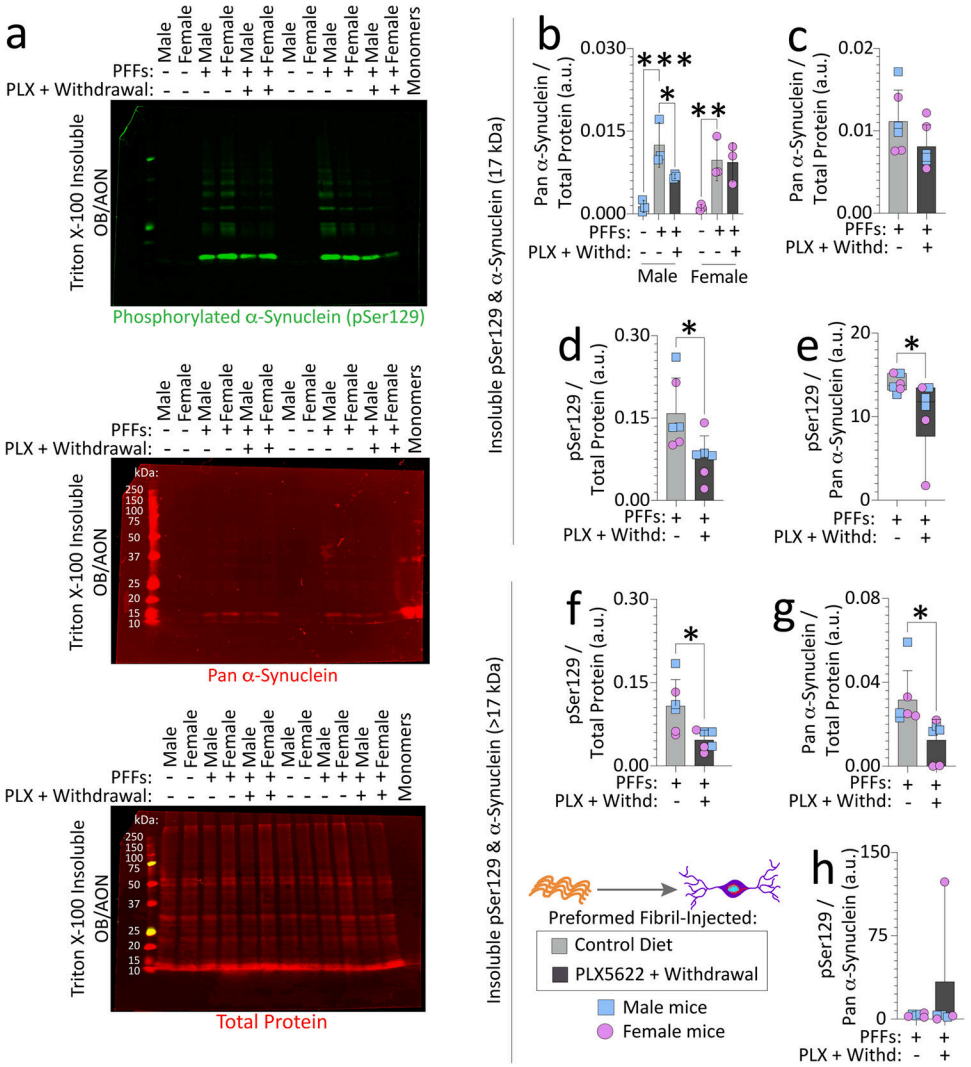

Fig. 3. Transient exposure to PLX5622 (2-weeks “ON” and 7-weeks “OFF”) lowers nonionic detergent-insoluble phosphorylated and pan-α-synuclein in the OB/AON of preformed fibril-injected aged mice.

Aged, outbred CD-1 mice of both sexes were fed special chow with or without the CSF1R inhibitor, PLX5622, for two weeks, and then fed standard rodent chow for an additional 7 weeks (timeline in Fig. 1a). Preformed fibrils (PFFs; 5 μg in 1 μL) were injected into the bulbar anterior olfactory nucleus (OB/AON) seven days after initiation of the PLX5622 diet. OB/AON tissues from PFF-injected aged mice fed control chow or transiently exposed to the PLX5622 diet were sequentially extracted to obtain nonionic, detergent-insoluble fractions, and subjected to immunoblotting to probe for pSer129 and pan-α-synuclein (Volpicelli-Daley et al., 2014). OB/AON tissues from PBS-injected aged mice were included as controls and wild-type mouse α-synuclein monomers were loaded in the last lane to evaluate antibody specificities (**a**; higher-resolution image of the blot is in Fig. S8a). Note that monomeric α-synuclein migrates at ~16–17 kDa through denaturing gels, based on immunoblot in **a** and (Anderson et al., 2006; Sharon et al., 2001). Insoluble pSer129 and pan-α-synuclein bands at 17 kDa were quantified (**b-e**) separately from bands of higher

molecular mass (> 17 kDa; **f-h**) and expressed as a fraction of the Total Protein Stain as a loading control. Levels of insoluble pSer129 were also expressed as a fraction of pan-α-synuclein in **e** and **h**. Additional data from these experiments are shown in Fig. S8. For studies in Figs. 3 and S8, three murine OB/AON samples had to be collapsed into one. Each group has three dots/statistical units, but data were generated from nine mice per group (see Methods). Shown are group means + SDs or box plots with interquartile ranges. $*p \leq 0.0500$, $**p \leq 0.0100$, $***p \leq 0.0010$; Mann-Whitney U (boxplots in **e, h**), unpaired t-test (**c-d** and **f-g**), or two-way ANOVA/Bonferroni (**b**). All testing was two-tailed.

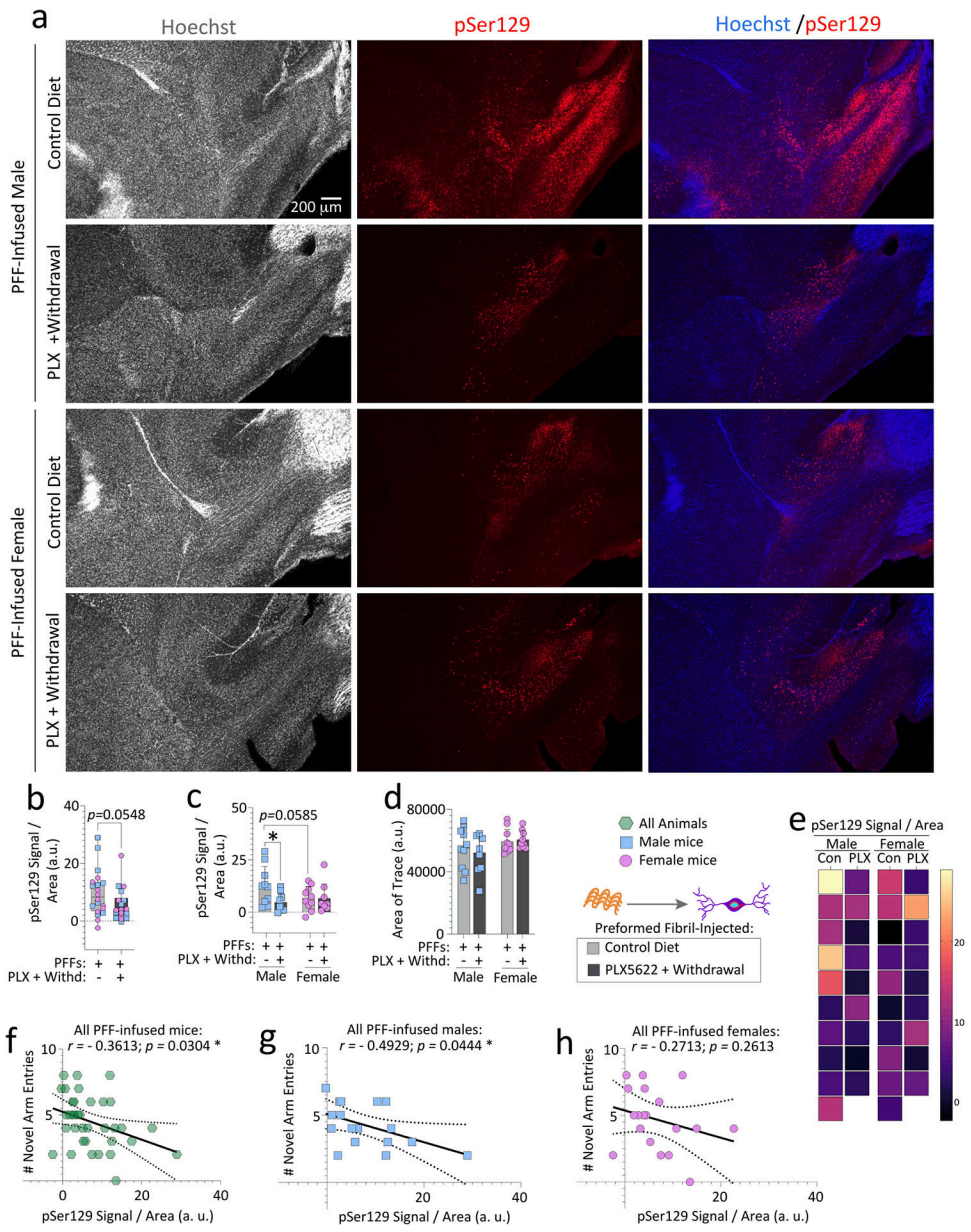

Fig. 4. Transient exposure to PLX5622 (2-weeks “ON” and 7-weeks “OFF”) reduces phosphorylated α-synuclein in the olfactory peduncle of preformed fibril-injected aged male but not female mice.

Aged, outbred CD-1 mice of both sexes were fed special chow with or without the CSF1R inhibitor, PLX5622, for two weeks, and then fed standard rodent chow for an additional 7 weeks (timeline in Fig. 1a). Preformed fibrils (PFFs; 5 µg in 1 µL) were injected into the bulbar anterior olfactory nucleus seven days after initiation of the PLX5622 diet. Brain sections were subjected to Tyramide Signal Amplification to improve the signal-to-noise ratio of the pSer129 immunolabel, scanned on an Odyssey Imager M at a resolution of 5 µm, and the olfactory peduncle (Brunjes et al., 2011) was outlined to obtain the pSer129 signal. pSer129 signal was then divided by the area of each trace (**b-d**). Representative photomicrographs of Hoechst-stained and pSer129-immunolabeled anterior olfactory nuclei

are shown in **a**. Heatmap depicting the pSer129 signal per unit area of the olfactory peduncle from all mice is in **e**. Correlation analyses of the numbers of novel arm entries (from the Y-maze forced alternation test shown in Fig. 2) with the pSer129 signal in the olfactory peduncle of all PFF-infused mice (**f**) or of PFF-infused males *vs.* females (**g-h**). Note that two mice were excluded from the Y-maze and inclusion assays due to dermatitis and abdominal abscesses (see Methods). In addition, mice that made less than three arm entries during the first minute of the second Y-maze trial were also excluded from the behavior correlations (see SI Methods and (Wolf et al., 2016)). Each mouse is illustrated as a colored dot on bar graphs with group means + SDs, on box plots with interquartile ranges, or in scatterplots for correlations. $*p \leq 0.0500$; Mann-Whitney U (boxplot in **b**) or two-way ANOVA/Bonferroni (**c-d**). Pearson correlation analyses are shown in **f-h**. All testing was two-tailed.

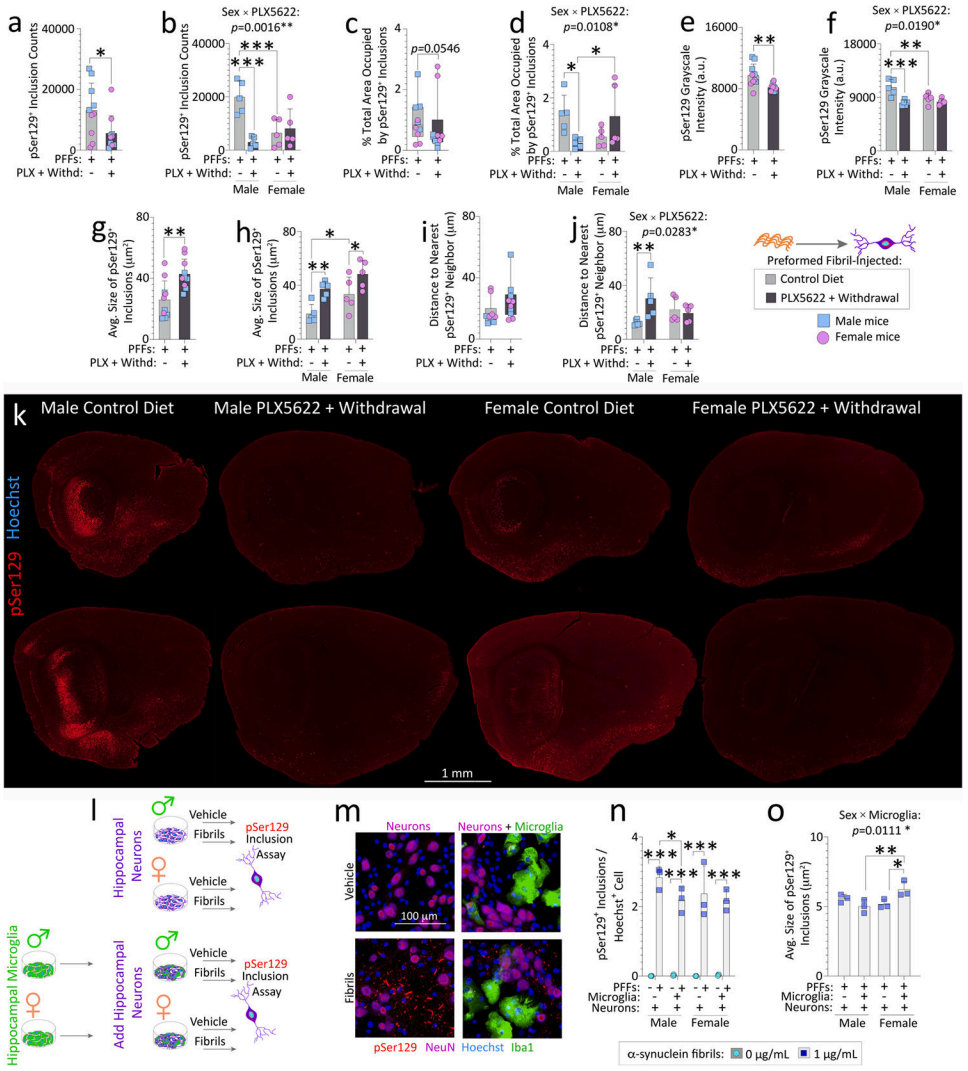

Fig. 5. Sex-specific regulation of pSer129$^+$inclusion numbers and sizes in PFF-injected aged mice after transient PLX5622 exposure (2-weeks "ON" and 7-weeks "OFF").

Aged, outbred CD-1 mice of both sexes were fed special chow with or without the CSF1R inhibitor, PLX5622, for two weeks, and then fed standard rodent chow for an additional 7 weeks (timeline in Fig. 1a). Preformed fibrils (PFFs; 5 μg in 1 μL) were injected into the bulbar anterior olfactory nucleus seven days after initiation of the PLX5622 diet. Brain sections from PFF-injected aged mice (n = 5 randomized mice per group) were subjected to Tyramide Signal Amplification of the pSer129 signal and scanned on a VS200 Olympus imager (**a-k**). pSer129$^+$ inclusions in the entire lateral limbic rhinencephalon were quantified *via* True AI/Deep Learning (Olympus) to identify the numbers of pSer129$^+$ inclusions (**a-b**), % total area (area fraction) occupied by pSer129$^+$ inclusions (**c-d**), mean grayscale intensity of pSer129$^+$ inclusions (**e-f**), average sizes of the individual pSer129$^+$ inclusions (**g-h**), and the distance to the nearest pSer129$^+$ neighbor (**i-j**). Representative photomontage of the pSer129 staining (**k**; for higher resolution image and Hoechst labeling, please download Fig. S9). Young primary hippocampal neurons from male or female rat pups were cultured with or without sex-matched primary hippocampal microglia (**l-o**). Neurons and neuron/glia

cocultures were exposed to vehicle or PFFs for 10 d. pSer129^{+} inclusions were expressed as a fraction of Hoechst^{+} cells (**n**). Average sizes of pSer129^{+} inclusions (**o**). Intervariable statistical interactions are shown above respective graphs. Each mouse (or each *in vitro* culture from one litter of pups) is illustrated as a colored dot on bar graphs with group means + SDs or on box plots with interquartile ranges. $*p \leq 0.0500$, $**p \leq 0.0100$, $***p \leq 0.0010$ for indicated comparisons; two or three-way ANOVA/Bonferroni (**b, d, f, h, j, n-o**), Mann-Whitney *U* (**c, i**), unpaired *t*-test (**a, e, g**). All testing was two-tailed.

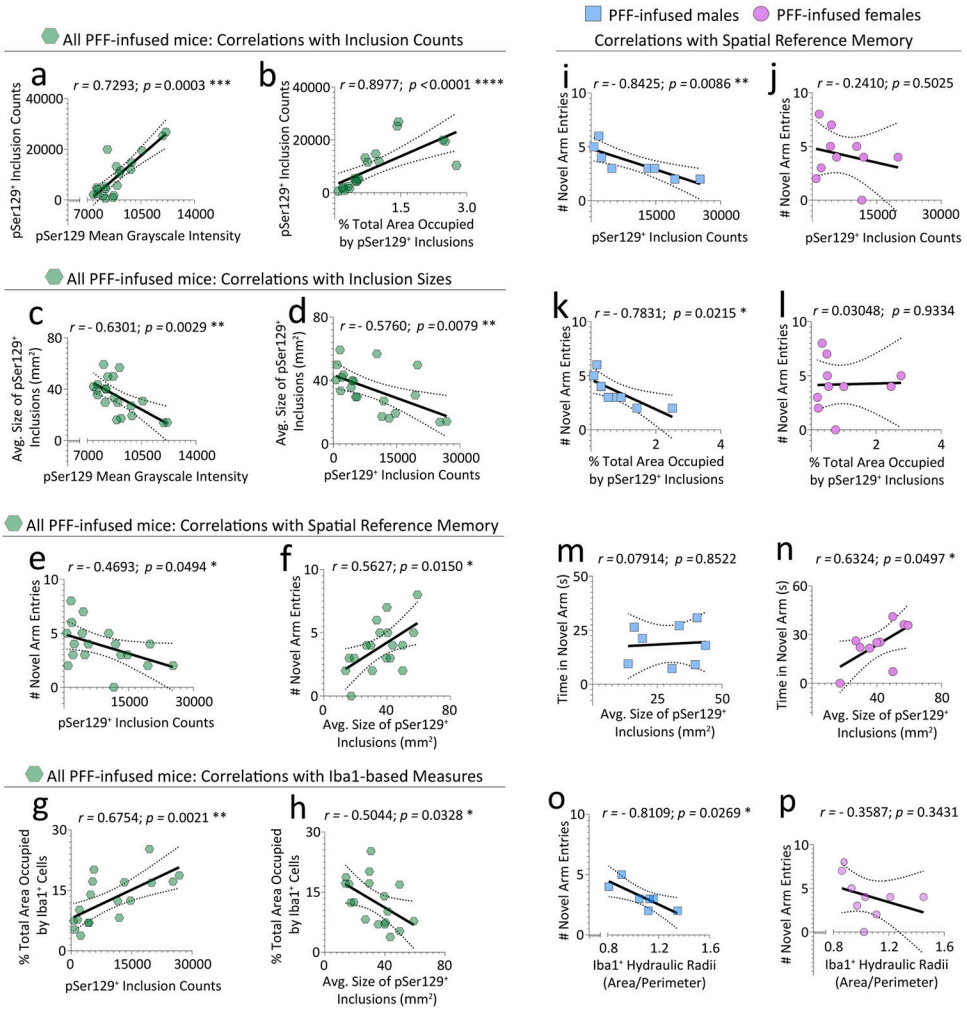

Fig. 6. Correlations between spatial reference memory, Iba1$^+$cells, and pSer129$^+$inclusions.

pSer129$^+$ inclusion morphology data from Fig. 5 were tested for correlations to assess the consistency of the AI/Deep Learning, or with data from the Y-maze forced alternation test in Fig. 2. In addition, Iba1$^+$ cell morphology data from Fig. S10 were tested for correlations with pSer129$^+$ inclusion morphology data from Fig. 5 or with data from the Y-maze forced alternation test in Fig. 2. Inclusion counts were positively correlated with mean grayscale intensity of the pSer129 label (**a**) and with the total area occupied by the inclusions (*i.e.,* area fraction; **b**). Average sizes of pSer129$^+$ inclusions were negatively correlated with mean grayscale intensity of the pSer129 label (**c**) and with inclusion counts (**d**). Number of novel arm entries were negatively correlated with inclusion counts (**e**), but positively correlated with average inclusion sizes (**f**). The total area occupied by Iba1$^+$ cells (*i.e.,* area fraction) was positively correlated with pSer129$^+$ inclusion counts (**g**), but negatively correlated with the average sizes of individual pSer129$^+$ inclusions (**h**). The negative correlation between novel arm entries and inclusion numbers was mainly attributed to male (**i**) and not female (**j**) mice. The area fraction of the inclusions was also negatively correlated with novel arm entries in male (**k**), but not female (**l**) mice. Time spent in the novel arm was correlated with average sizes of pSer129$^+$ inclusions in females but not males (**m-n**). Hydraulic radii of

Iba1^{+} cells were negatively correlated with novel arm entries of PFF-infused male mice only (**o-p**). Note that additional correlation data are shown in Fig. S13. Each mouse is illustrated as a colored dot on the scatterplots. $*p \leq 0.0500$, $**p \leq 0.0100$, $***p \leq 0.0010$, $****p \leq 0.0001$; Pearson correlation analyses in **d-p**, and Spearman correlation analyses in **a-c** (*i.e.*, failed the Shapiro-Wilk test for normality). All testing was two-tailed.